Carbon membranes performance for water removal in DME synthesis via membrane reactor

Basile, G.

Award date:
2021

EINDHOVEN UNIVERSITY OF TECHNOLOGY

Department of Chemical Engineering and Chemistry
Chemical and Process Technology

Carbon membranes performance for water removal in DME synthesis via membrane reactor

Master thesis

Gaia Basile, s1347594

Supervisors

Prof. Dr. Eng. Fausto Gallucci
Dr. Fernanda Neira d'Angelo
M.Sc. Serena Poto

Committee

Prof. Dr. Eng. Fausto Gallucci
Dr. Fernanda Neira d'Angelo
Dr. Antoni Forner Cuenca
M.Sc. Serena Poto

Eindhoven, 11th December 2020

Abstract

In the last decades, as fossil fuels consumption increased, the global warming became of great concern. The impact of the rising earth temperature is caused by greenhouses gases emissions, mainly CO2. Among several solutions, Carbon Capture and Storage (CCS) arose interest in both research and industry, as a practical short-term solution that can be implemented in pre-existing plants. The next step to CCS would be the CO2 utilization, as it can be used as a low-cost reactant, due to its large availability, to synthetize valuable chemicals. One of the chemicals that can be produced from this gas is DME, a volatile organic compound that can be used both as a diesel substitute in current engines and energy carrier. However, its synthesis from CO2 is severely affected by thermodynamic limitation, which results in low DME yield.

Water is the main by-product of these reactions and its removal can potentially increase CO2 conversion and the DME yield, shifting the equilibrium towards DME production. In order to effectively remove water from the reaction zone, a membrane reactor can be used. In this way, water can be continuously removed as it is produced. This concept is not new to research and zeolite membranes have been already tested for this purpose. However, the acidity of zeolite membranes makes them unstable in hot and humid environment. Moreover, it is difficult to produce a crack-free membrane that can be used for industrial application.

Carbon molecular sieve membranes (CMSMs) were considered as a suitable alternative to zeolites, as they have high chemical and thermal stability. Their hydrophilicity can enhance water permeation and their ultramicropores can increase their selectivity towards the gases. However, the membrane properties of carbon membranes can significatively vary, depending on their synthesis methodology.

In this study, two carbon membranes, carbonized at different temperature, were characterized and tested in order to evaluate their performance. Permeance and selectivity were measured experimentally and implemented in a 1D-isothermal-membrane reactor model, which predict their performance in both the direct and indirect DME synthesis.

In this study we found that the membrane structure, thus the membrane performance, is affected by the different carbonization temperature. In particular, the carbonization temperature influences the membrane pore-size and hydrophilic behaviour. Moreover, a higher CO2 conversion and DME yield was reached by the model compared to the conventional production methods, in both direct and indirect process.

Lastly, we highlighted room for improvement on carbon membrane synthesis, so that they can be successfully implemented for industrial purposes in the future.

Contents

List of Figures

List of Tables

List of Symbols

A	phenomenological coefficient
A_m	membrane area
D_{mo}	membrane outer diameter
D_{si}	reactor shell inner diameter
ΔP	Pressure difference acting on the membrane
ΔP_{ML}	Logarithmic mean pressure gradient between permeate and retentate
ΔH_0	standard heat of reaction
ε	catalyst bed porosity
E_a	activation energy
F	molar flow rate
Φ	volumetric flow rate
J	trans membrane flux
k_1	kinetic constant of reaction 1
k_2	kinetic constant of reaction 2
k_3	kinetic constant of reaction 3
K_{p1}	equilibrium constant of reaction 1
K_{p2}	equilibrium constant of reaction 2
K_{p3}	equilibrium constant of reaction 3
K_{CO_2}	CO_2 adsorption constant
K_{CO}	CO adsorption constant
K_{H_2}	H_2 adsorption constant
K_{H_2O}	H_2O adsorption constant
m	mass of liquid collected
MW	molecular weight
N_r	number of reactions
P	pressure
P_0	saturation pressure
P_k	capillary condensation pressure
$\wp_i$	permeance of a generic component *i*
ρ	density of gas
ρ_c	density of catalyst
r_p	membrane pore radius
r	reaction rate
R	ideal gas constant
σ	interfacial tension
S_i	selectivity of generic component *i*
ϑ	contact angle
T	temperature
T_{carb}	carbonization temperature
Δt	duration of the experiment
v	superficial gas velocity
X	generic driving force
x	x coordinate perpendicular to the membrane

Superscripts

R	reaction zone
P	permeation zone

Subscripts

i,j generic species

0 inlet conditions

Chapter 1
Introduction

Worldwide, fossil fuels represent the main source of energy. The fossil fuels consumption increased exponentially in the last century, causing an increase in greenhouses gas emissions. [1] Consequently, the superficial temperature of the planet also increased, causing several problems. This increase in temperature is currently well known as global warming.

The global warming is raising major concern among both the scientific community and the global population, which demands for practical solution to avoid irreversible damage to the planet. [2] In this scenario, industries are blamed the most, as responsible for a large volume of CO_2 emission. Indeed, carbon dioxide plays a key role in the greenhouse effect, being the first responsible for global warming. Today, the environmental impact of CO_2 emissions into atmosphere is known and understood. [2]

Therefore, limiting the amount of CO_2 emitted into atmosphere represent a practical short-term solution to the problem. Among the possible solutions, Carbon Capture and Storage (CCS) technologies awoke the interest of both scientists and industries. CCS strategy describes a series of operation ranging from CO_2 separation to its storage. [3] These technologies are especially attractive for their feasibility in CO_2 emission reduction from different sources, as power generation and natural gas processing. [4]

However, after being captured, CO_2 becomes a waste to storage, and it is likely that a large amount of CO_2 will be stored in the future. If the wasted CO_2 could be used as a reactant for the production of chemicals or fuels, it could be converted in a new energy source. As a result, the large amount of stored CO_2 would be turned to a low-cost reactant. Centi et al. [5] reported that, since the fuel market is larger than chemicals, the most advantageous route would be the reconversion of CO_2 into valuable fuels. They also reported that Methanol and Dimethyl ether (DME) are the preferred choice, the latter being more interesting as it is a higher value energy carrier.

DME is a volatile organic compound with similar properties to LPG (liquid petroleum gas), although it is non-cancerogenic and non-toxic. [6] Due to the similar behaviour to LPG and to its high cetane number, DME is considered a valuable and cleaner fuel alternative for current diesel engines. [7],[8] Moreover, it is a suitable solution to H_2 transport, being an excellent energy carrier, as it has a high energy density and high H/C ratio. [9] Currently, DME is mainly

produced from syngas via two different processes, commonly called direct and indirect route. In the direct process, DME is synthetized in one step reactor, whereas in the indirect route the feedstock is first converted into methanol in one reactor and then methanol is dehydrated into DME in a second reactor.

The main drawback of DME production from a CO_2/H_2 feed is that the process is thermodynamically limited. The independent reactions involved in the DME production process, starting from a CO_2/H_2 mixture, are the following:

$$CO_2 + 3H_2 \rightleftarrows CH_3OH + H_2O \qquad \Delta H_0 = -49.5 \text{ kJ/mol} \qquad Eq.\ 1$$

$$CO_2 + H_2 \rightleftarrows CO + H_2O \qquad \Delta H_0 = +41.2 \text{ kJ/mol} \qquad Eq.\ 2$$

$$2CH_3OH \rightleftarrows CH_3OCH_3 + H_2O \qquad \Delta H_0 = -23.4 \text{ kJ/mol} \qquad Eq.\ 3$$

From the standard enthalpies of reaction in *Eq.1*, *Eq.2* and *Eq.3*, it is possible to see that the process is overall exothermic, therefore low temperatures favor the desired product formation (i.e. Methanol and DME). Moreover, all the reactions are limited by thermodynamic equilibrium.

A key issue in this process is water formation, which decrease the thermodynamic limit even further with respect to conventional syngas route. Water is a by-product of all the reactions, which inhibits methanol formation and its subsequent dehydration to DME. Moreover, water can decrease the catalyst activity by 1) adsorbing on the acid active sites on which methanol should decompose to produce DME [10] and 2) by changing the morphological structure of the catalyst. [11] If water can be selectively removed from the reaction zone, the production of the desired product would increase, as stated in Le Chatelier's Principle. With this solution, it would be possible to overcome the thermodynamic limitation and boost DME production.

A promising technology for this purpose is the membrane reactor. A membrane reactor is a unit in which reaction and separation occur at the same time, by means of the integration of a membrane in the catalytic bed. Theoretical studies already showed that the product yield can greatly improve by implementing a membrane reactor in thermodynamically limited processes. [12], [13] With the right membranes, high amount of water can be removed from the reaction environment. Therefore, the membrane choice plays a key role for the selective water removal.

Carbon membranes may be a valid candidate for this process due to their hydrophilic behaviour and high chemical and mechanical stability. Although these membranes are more expensive when compared to organic polymeric membranes, they show higher permeability and selectivity. [14] Nonetheless, although carbon membranes are widely studied for gas separation application, due to their molecular sieving properties, they have not yet been intensively studied for water removal and vapor permeation.

Carbon membranes' hydrophilic behaviour was first observed in gas permeation studies: a decrease in gas permeance was noticed for membranes exposed to humid environments. This was attributed to the presence of functional groups on the membrane surface. [15]

However, what it is considered a drawback in gas separation, may represent a solution for this system, as the presence of water may reduce the loss of reactant by blocking or reducing the gas permeation through the membrane.

Aim of the project

In this project, the feasibility of inorganic carbon molecular sieve membranes (CMSMs) for DME production from CO_2 and H_2 was tested at laboratory scale. The aim of the study was to investigate if carbon membranes can improve the DME yield when used in a fixed bed membrane reactor. In order to do so, CMSMs were tested for water and methanol vapor permeation and water vapor/gas separation in different operating conditions. The influence of carbonization temperature on both the membrane performance (permeability and selectivity) and the membrane structure was studied. To support the study, a phenomenological membrane reactor model was used to simulate two routes of DME production, to understand whether the tested membranes could be used to boost one route more than another.

Membrane performance can be influenced by its structure. Thus, to understand how the membrane structure can influence the water removal and the surface interaction with all the molecules involved in the reaction scheme, two membrane sample film carbonized at 600°C and 700°C were characterized. The information of interest was the pore size distribution, the surface functional groups still present and the water and gas adsorption on the membrane surface. Then, permeance of water and methanol were experimentally evaluated via permeation test for both membrane sample, and ideal selectivity was computed. Lastly, real selectivity of water and gas mixture was derived experimentally. These results were implemented in a 1D-phenomenological membrane reactor model and the results were compared to traditional reactor with thermodynamic limitation, in order to demonstrate that carbon membranes can represent a promising solution to increase DME yield. A comparison between direct and indirect process was also simulated, to understand which route would be the preferred one.

A more detailed theoretical background is presented in Chapter 2, which explains the fundamentals of carbon membranes and the theory necessary to understand the next chapters. In Chapter 3, the experimental setup and methodology are explained in detail, illustrating the experimental procedure and the mathematical model used in the project. In Chapter 4 results are presented and discussed, for both the experimental work and the simulation. Lastly, in Chapter 5, conclusion is presented as well as an outlook on the subject and the study. In this last chapter, the most important findings are summed up.

Chapter 2
Theoretical Background

1. Membrane technology

Membrane technology is gaining importance in the last decades as a more environmentally friendly alternative to conventional separation units. Already widely used for various application, as water purification and gas separation, membrane separation is a less energy demanding process, which helps to reduce the separation costs while reducing the environmental impact of the separation process. [16]

A membrane is defined as a semi-permeable barrier, which can selectively promote the passage of one or more component of a mixture. Therefore, at the outlet of a membrane system, two streams are present: the permeate, which is the stream containing all the species that were able to pass through the membrane, and the retentate, which contains the retained compounds. The permeation of specific compound is driven by a pressure, concentration, temperature or chemical potential gradient. Depending on the driving force, the separation may depend on the physical properties of the compounds of the feed, or on their chemical interaction, or both. However, the degree of the separation depends on the membrane structure and material.

The main parameters used to assess the membrane performances are permeability and selectivity. Permeability represents the capability of a specific molecule to pass through the membrane. The selectivity compares the permeability of two different components to understand which one permeates more easily through the membrane. The rate at which the species permeate through the membrane can be correlated to the driving force through its flux, as expressed in the following equation:

$$J = -A\frac{dX}{dx} \qquad \textit{Eq. 4}$$

Where A is the phenomenological coefficient, and *dX/dx* is a generic driving force expressed on the x coordinate, perpendicular to the membrane. Depending on the membrane structure, the flux equation can be expressed as Fick's law of diffusion or Darcy's law through porous media. The first case applies when dealing with a dense membrane structure, in which the

permeation of the molecules is driven by a concentration gradient and the transport mechanism is well described by the solution-diffusion model. Darcy's law is used when the driving force is a pressure gradient, and the membrane has a porous structure, in which the molecules follow the pore-flow model. Beside the membrane structure classification (porous and dense), they can also be classified depending on which material the membrane is made of. The two main categories are organic and inorganic membranes: the first being mainly composed by polymeric membranes, which are also the most commonly used nowadays. In the second category, membrane made from metals, glass, zeolites and carbon are included. [14]

2. Inorganic membranes

Currently, inorganic membranes are mainly used for energy-related purposes. [14] They can be divided in two main groups: dense and porous membranes. Porous inorganic membranes can also be divided in two subcategories: symmetric and asymmetric. Symmetric membranes are composed by a single material and have a single morphological structure. Asymmetric membranes have multiple morphological structures on different planes, each one having a specific pore size. [17] Dense inorganic membranes are mainly used for hydrogen and oxygen gas separation, whereas inorganic porous membranes are used when gas with similar size must be separated from gaseous mixtures, due to their sieving properties [14]. These membranes are more common in industrial applications than dense membranes, as they show higher permeability. Furthermore, even if the production process is more expensive than polymeric membranes, the inorganic membranes have the advantage to reach higher permeability and selectivity, and to be more thermally and chemically stable, when compared to the polymeric ones. [18]

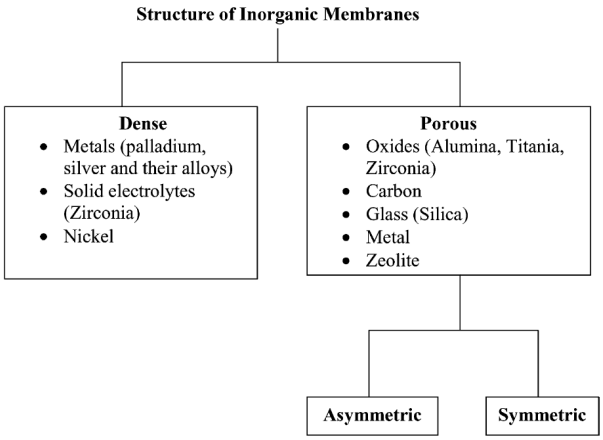

Figure 1: Schematic representation of inorganic membranes classification [14]

In gas separation, inorganic porous membranes are mainly used, due to the already mentioned advantages. In this category, zeolites membranes arise particular interest due to potentially high performances for industrial applications. [19]

Zeolites membranes are membranes with a well-defined, microporous, crystalline structure, containing silica, alumina and oxygen in their framework. [17]These membranes show good stability at high temperatures and high selectivity. [5],[13] However, zeolite membranes are sensitive to cracking when produced for large scale application, which makes it difficult the scale up when used in membrane reactors. [20] Moreover, the presence of cracks in their structure causes a decrease in their performance. Another cause of decrease in performance of zeolite membranes is the sensitivity to water of their acid sites. For these reasons, zeolite membranes are not the best candidate for water removal purposes.

Another promising choice for gas separation and, potentially, also for water removal, are inorganic carbon membranes. These membranes have been widely studied for gas separation due to their molecular sieve mechanism. However, a drawback of these membranes in gas separation is their hydrophilicity. Nonetheless, this affinity towards water may be beneficial for in situ water removal. Contrary to zeolite membranes, carbon membranes have not yet been intensively studied for water removal applications.

3. Carbon membranes

Carbon membranes are porous inorganic membranes, which are produced via carbonization of an organic precursor, within a thermal decomposition called pyrolysis. [21] These membranes show high separation capability, high thermal and chemical stability, which makes them a suitable candidate for industrial application. [18] Carbon membranes have shown much higher selectivity compared to polymeric membranes, as they can also act as sieves. [22], [23]. The molecular sieving mechanism, combined with adsorption, permits to easily separate gas molecules with almost identical size. [24]

3.1. Preparation of carbon membranes

Carbon membranes can be supported or non-supported. Usually, supported carbon membrane are preferred to the non-supported ones, due to a better mechanical stability, which makes them appropriate for industrial applications. [25]

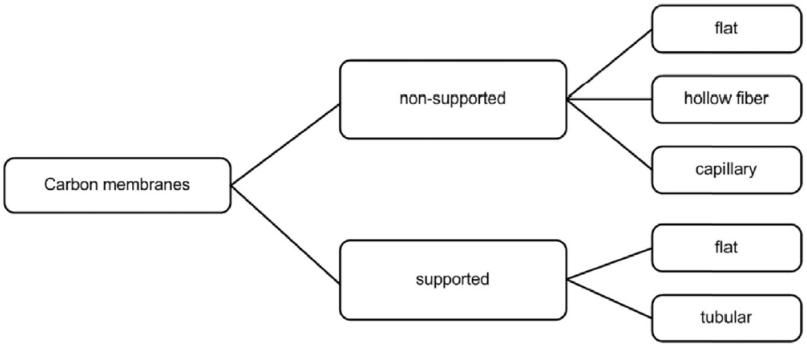

Figure 2: Carbon membrane classified by configuration [18]

Supported carbon membranes are prepared by coating a support with the polymeric precursor, which can be made from ceramic or metallic material. Ceramic support are less robust compared to metallic ones, however they have a better surface quality, which allows to produce a thinner membrane layer. [26] The support can also increase the permeance of the membrane, due to larger pores compared to the carbon layer. On the other hand, the gas permeance and the microstructure of the carbon membrane is determined by the polymeric precursor used during the fabrication, the fabrication process itself and the pyrolysis condition. [25]

The precursor should satisfy precise conditions: the polymeric precursor should have high carbon yield after pyrolysis and thermosetting properties. Some of the most used precursor are: PFA, PVDC, cellulose acetate and phenolic resins. [18] Phenolic resins are a promising candidate as they are commercially available, they have a high carbon yield and their cost is quite low. [27] Moreover, carbon membranes made from phenolic resin have shown good performance even with a single-step coating. [25],[27] This may not be always the case, as to obtain a defect-free membrane the coating may need to be repeated several times. [24]

After the precursor is coated in a thin layer on the membrane support, which is usually made of α-Al_2O_3, the membrane goes under thermal treatment, that can range between 500°C-1000°C, in vacuum or inert atmosphere [25]. The heating rate is controlled and depends on the precursor, as well as the treatment time. The temperature at which the membrane is treated during this step is called carbonization temperature and has a direct effect on the membrane structure and performance. Indeed, depending on the temperature at which the membrane is carbonized, different atoms group are removed from the precursor, affecting the microstructure of the carbon layer. Generally, the higher the carbonization temperature, the less similarity can be found between the final membrane structure and its precursor. [18] The amount of atom group removed from the carbon layer during pyrolysis can affect the membrane hydrophilicity, as it strictly depends on the oxygen-containing surface groups. [15] Furthermore, the carbonization temperature also affects the pore size distribution of the carbon layer, as it is responsible for the changing in the morphological structure of the selective layer. Indeed, it has been observed that the pores start to appears at T_{carb}=500°C, they enlarge up to T_{carb}=700-800°C and shrinks at T_{carb}>800°C, with the best performance obtained at T_{carb}=700°C for gas separation. [28].

3.2. Transport mechanism through carbon membranes

Transport mechanism through carbon membranes for vapor permeation and water removal is still under studies and not well understood. However, the transport mechanism has been intensively studied for gas separation from gaseous mixtures and it depends on the difference between the membrane pore size and the gas molecule size.

Carbon membranes show a binodal pore size distribution, with both ultramicropores and micropores, as shown in Figure 3:

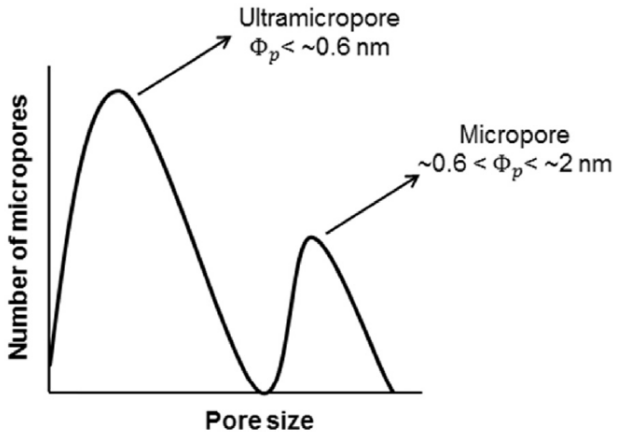

Figure 3: Pore size distribution trend for carbon membranes. [18]

Both micropores and ultramicropores contributes to determine the transport mechanism through the membrane, accounting for two different contribution. Within the microporous structure, sorption takes place, whereas in the ultramicroporous structure, the predominant transport mechanism is molecular sieving. [18] This combination of both micropores and ultramicropores guarantee both high permeance and high selectivity in carbon membranes. However, other transport mechanisms are involved in gas permeation, even though molecular sieving is the predominant one.

Particularly, four different mechanism best describes the gas permeation through carbon membranes: viscous flow, Knudsen diffusion, selective adsorption-surface diffusion and molecular sieving (Figure 4). Depending on the pore size distribution, one or more of these mechanisms may dominates the overall transport.

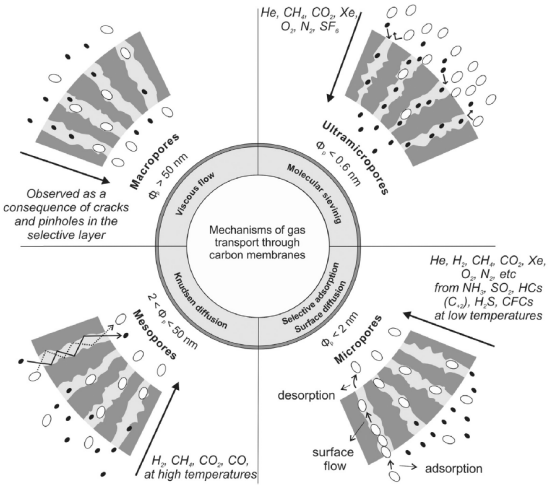

Figure 4: Main transport mechanisms in gas separation using carbon membranes. A schematic representation. [18]

When viscous flow is detected during gas permeation, it indicates that the membrane has fabrication defects. In case of viscous flow, the permeate flux of gases is rather high, causing an increasing of the gas permeability. On the other hand, as the defects are in the order of macropores, the selectivity is very low. If permeance is increasing with increasing pressure, then it is proven that viscous flow is the predominant transport mechanism and the membrane has cracks. [18]

When the mean free path of the molecule is higher than the mean pore diameter of the carbon membrane, Knudsen diffusion occurs. In this case, the permeation rate of each gas molecule is inversely proportional to the square root of their molecular weight. [29] However, the selectivity obtained when this mechanism takes place in gas separation, are quite low and they are not really practical. [18]

Another mechanism that may occur in carbon membranes is the selective adsorption-surface diffusion, which consists in the permeation of non-adsorbable gases from the one which can adsorb on the membrane surface. [14] This mechanism is generally coupled with other mechanisms, such molecular sieving or Knudsen diffusion and it is affected by temperature: low temperatures enhances the gas adsorption on the membrane surface. When this mechanism is present, high selectivities are possible due to the restriction of the pore size caused by the presence of the adsorbed molecules on the pores walls. [18]

Lastly, the predominant transport mechanism, as already mentioned is molecular sieving. Carbon membranes have pores with relatively wide openings and with corresponding narrow constrictions. These constrictions are similar in size to the molecular size of gaseous molecules, thus it is possible to effectively separate gases by tuning the dimension of these constrictions, even when they have a similar molecular diameter [14] For this reason, larger molecules are retained as they are not capable to pass through the pore. Moreover, when the pore size is sufficiently small compared to the molecule size, repulsive forces dominates, and activation energy is required to diffuse. Therefore, it is possible to separate molecules with similar size, based on the energy needed to pass through. [18]

3.3. Capillary condensation

Until now, gas transport mechanisms were presented. However, when dealing with condensable substances, as water in vapor form, another phenomenon starts to play a role, called capillary condensation. This mechanism plays a role in vapor permeation through small pores and it is not well described yet for a membrane system. [30] Capillary condensation is a mechanism in which vapors condensate in the membrane small pores due to a pressure change within the pores, approaching the partial pressure of the condensable gas. Usually, this phenomenon is the results of a multilayer adsorption on the pore walls, which reduce the pore size, therefore a change in pressure is expected inside the pore. [31] When this pressure change reaches the saturation pressure, the vapor condenses into the pore, partially or completely, reducing the pore size even more. The pressure at which the vapor condensates within the pores is described by Kelvin equation, and it is function of the operating temperature. [32]

$$\frac{\rho RT}{MW} ln\left(\frac{P_k}{P_0}\right) = -\frac{2\sigma cos\vartheta}{r_p} \qquad Eq.\ 5$$

where *MW* the molecular weight, ρ the density of the condensed phase, P_0 is the saturation pressure for a planar phase, P_k the capillary condensation pressure, σ the interfacial tension, r_p the pore radius and ϑ the contact angle.

It is difficult to predict how condensation happens within the pore of a membrane, although Lee et al. [32] presented six different flow models, shown in Figure 5. They six cases reported are described as:

1) in the first case, the flow is described by a combination of Knudsen diffusion and surface diffusion,

2) in the second case, capillary condensation dominates close to the pore entrance, whereas surface diffusion dominates towards the end,

3) the third case is the one in which only capillary condensation is happening,

4) in the fourth case, the upstream end of the pore is filled with condensate and no force acts on that side.

5) The upstream end of the pore is in the same condition as 4), however, capillary condensation is happening downstream.

6) In the sixth and last case, the pore is completely filled with bulk condensate with no meniscus present.

However, these cases do not describe accurately capillary condensation in the membrane pores. The reason being that the membrane pores are not perfectly cylindrical, as Lee et al. assumed. Moreover, the pore size in inorganic membranes is not uniform, as already stated in the previous sections. [30]

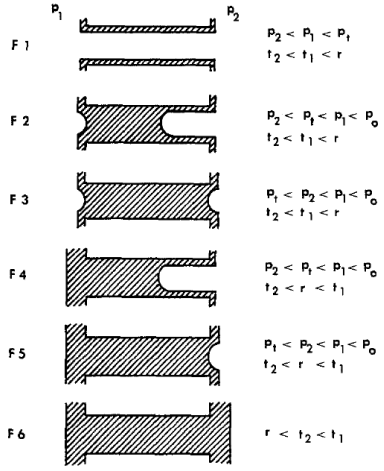

Figure 5: Flow models for capillary condensation in small cylindrical pores. [32]

Although the description of the phenomenon is still under investigation, the effects of capillary condensation on gas permeance is known. Indeed, due to the liquid blockage, gas permeation decreases drastically, reaching very high selectivity with respect to the condensable vapor. [33] Moreover, the permeance of the condensable vapor also increase, due to the interaction between the molecules in vapor phase with the one on the liquid films that forms in the pore is increasing. This effect makes these types of membrane valuable candidates for water removal from a slightly superheated stream.

4. DME production

Dimethyl ether (DME) is a volatile organic compound, which can be easily stored as liquid when pressurized above 0.5MPa, with similar properties to LPG (liquid petroleum gas). [6], [34] For example, DME and LPG have similar vapor pressures, which enable DME to be stored and transported in already existing LPG infrastructures. [35] Due to their similarities, DME is regarded as a promising alternative fuel, especially in already existing diesel engines. Furthermore, it can be used as a household gas and as a more environmentally friendly refrigerant and aerosol, due to its zero-ozone depletion potential compared to traditional refrigerants. [36]

DME is considered a greener fuel compared to petroleum derived fuels and natural gas for different reasons. Firstly, since DME has no C-C bonds and contains about 35% oxygen, unburned hydrocarbons and carbon monoxide content in combustion products is lower than natural gas. [34] Moreover, it has a higher cetane number than diesel, which makes DME an alternative to current fuels with little to no emission of NO_x and particulate matter. [37] However, the heat value of DME is lower than diesel, which means that higher amount of DME is needed to reach the same power output. [37]

DME is currently produced via syngas, which can be be produced by a variety of feedstocks, ranging from coal and petroleum to natural gas and waste products. Currently, natural gas is the preferred feedstock for its large availability and the possibility to have a production cost independent of the oscillations in the oil price. [38]

DME can be produced via two different routes: the indirect and the direct route. In the first case, methanol is first synthetized from syngas (*Eq. 6* and *Eq. 7*). Then, methanol is purified and subsequently dehydrated into DME in a second reactor, over an acid catalyst (*Eq. 8*). As the overall indirect process is slightly exothermic, the methanol dehydration is favored by lower temperature, reducing by-products formation, such as coke. [36] Moreover, since the dehydration is an equilibrium reaction, both DME and H_2O inhibit methanol conversion to DME, as it can be seen in *Eq. 8*:

$$CO + 2H_2 \leftrightarrow CH_3OH_3 \qquad Eq.\ 6$$

$$CO_2 + H_2 \leftrightarrow CH_3OH + H_2O \qquad Eq.\ 7$$

$$2CH_3OH \leftrightarrow CH_3OCH_3 + H_2O \qquad Eq.\ 8$$

In case of direct route, methanol production and its subsequent dehydration to DME happen within the same reactor over a bifunctional catalyst. This means that equations 6, 7 and 8 happen in one step only. The overall process is highly exothermic, thus temperature control is important to avoid runaway reactions. [34] Moreover, water gas shift reaction must be considered in this process, which leads to CO_2 production as main by-product. Therefore, the following equation has to be added to the ones previously shown:

$$CO + H_2O \leftrightarrow CO_2 + H_2 \qquad \textit{Eq. 9}$$

Since all the reactions involved in the process are in equilibrium, the consumption of methanol during dehydration (*Eq.* 8) shifts the equilibrium towards the products, allowing for higher methanol production and, consequently, higher methanol conversion to DME. [34] Thus, direct process is preferred over the indirect process, as it allows for higher CO conversion and a simpler design, which leads to lower production costs compared to the two step methanol dehydration, even though the downstream separation of DME and CO_2 become difficult, especially when unconverted methanol is present. [39], [34]

However, a more interesting feedstock to produce DME would be CO_2. Carbon dioxide is currently regarded as a waste, which is emitted into atmosphere or stored underground. Using it as a reactant would transform a waste into a valuable low-cost source and would avoid CO_2 emission into atmosphere, reducing its impact on global warming. As already stated in Chapter 1, the main limit of using CO_2 as feedstock, instead of CO, is the high amount of water, which is not consumed through the WGS reaction. Indeed, when CO_2 is used as feedstock, the reverse water gas shift reaction happens in the system, generating even more water as byproduct of the overall reaction (*Eq.1, Eq.2, Eq.3*). A possible solution to shift the equilibrium towards the products, is the removal of water. Therefore, a membrane reactor is investigated as potential solution for the problem.

In a membrane reactor, a selective membrane towards water can be implemented. In this way, water permeates from the reaction zone to the permeation zone, where it is subsequentially removed from the reactor. By removing water, the equilibrium is shifted towards the products. However, the choice of the membrane should be carefully considered. Indeed, a membrane that inhibits gas permeation is needed, in order to avoid reactant or product loss, as H_2 or methanol.

It might happen that the membrane selectivity to methanol is low. In this case, when applied to the direct process, methanol permeates with water before having time to be converted into DME. In this scenario, there is a product loss, which is not desired. However, the low selectivity to methanol does not imply that the membrane cannot be used. Indeed, it might be that it has good performances in the indirect process. When used in the first step, water removal can increase methanol production, as well as methanol removal. Then, since methanol is separated from water between the first and the second stage, it can be recovered and fed in the second stage.

Chapter 3
Experimental

1. Carbon membranes

The carbon membranes studied in this project were provided by Tecnalia (Spain) and selected from different membrane samples after an initial screening. These membranes are characterized by an amorphous α-Al_2O_3 support and derives by the carbonization of a Novolac precursor. The precursor contains:

- Novolac-L 13% ;
- Formaldehyde 2.4%;
- Alumisol 0.8%;
- Ethylenediamine 0.6%;

Two membranes carbonized at two different temperature were selected, named 403-N and 405-N, with a carbonization temperature of 600°C and 700°C respectively. In this study, the membranes will be called CM600 and CM700 for readability purposes.

Figure 6: Carbon membranes tested. On top, 403-N at T_{carb} = 600°C. On bottom, 405-N, T_{carb}= 700°C.

The length of the carbon selective layer is between 11.5 and 13 cm, with an estimated film thickness of 4μm and a membrane area of $4.71 \cdot 10^{-3} m^2$.

2. Characterization

Carbon membrane films were provided by the company as well, as a fine powder was required for all characterization techniques. The carbon films provided by Tecnalia, were prepared in the same conditions of the membrane CM600 and CM700. The films were grinded to obtain a fine powder, ready to use for characterization purposes.

2.1. Nitrogen physisorption analysis

Surface area, pore volume and pore size distribution were determined by the nitrogen physisorption at 77 K, using a Tristar II 3020. The isotherms were elaborated according to the Brauner-Emmett-Teller (BET) method. Before the analysis, the samples were outgassed under vacuum conditions at 250 ºC for 4h to assure a clean surface. In these conditions, the humidity bounded to the surface evaporates and does not interfere with the physisorption analysis.

The basic principle on which is based the BET analysis is to evaluate the adsorption of a gas at constant temperature and different pressure, in order to create an adsorption isotherm. Since it is based on physical adsorption, the gas used should be inert and, therefore, nitrogen is usually used. The temperature at which the adsorption is conducted is the boiling point of liquid nitrogen. From the volume of adsorbed nitrogen, it is possible to calculate the pore size distribution of the sample.

2.2. Fourier Transformed Infrared Spectroscopy (FTIR)

To investigate the presence of residual functional groups after the carbonization process, the FTIR (Fourier Transformed Infrared Spectroscopy) analysis was performed. This technique is designed to identify inorganic and organic molecules bonds by means of infrared radiation containing different light frequencies. This radiation is sent to the sample, which, in turns, absorbs specific wavelengths, depending on which bonds are present in the material. The spectrometer measures both the wavelength and the corresponding intensity of the absorbed radiation. A spectrum is then generated according to a mathematical method called Fourier Transform. The wavelengths absorbed by the sample are characteristics of specific bonds. Therefore, the main functional group can be identified qualitatively. A quantitative information of the functional groups can be also derived from the peak intensity.

Before the analysis, the carbon film was grounded and diluted with KBr powder in order to obtain a 5wt% concentration. Then, a disc-shaped pellet was formed by applying a 10 kton force by means of a hydraulic press. A background spectrum was collected prior to each analysis, on a pure KBr pellet.

2.3. Thermogravimetric analysis

To gain insight into the membrane hydrophilicity and adsorption capacity, a thermogravimetric analysis (TGA) was performed on powder samples.

During a TGA analysis, the weight variation of the sample is recorded during time, as temperature and/or pressure changes, while feeding a gas. The P&ID of the setup used for such analysis is shown in Figure 7.

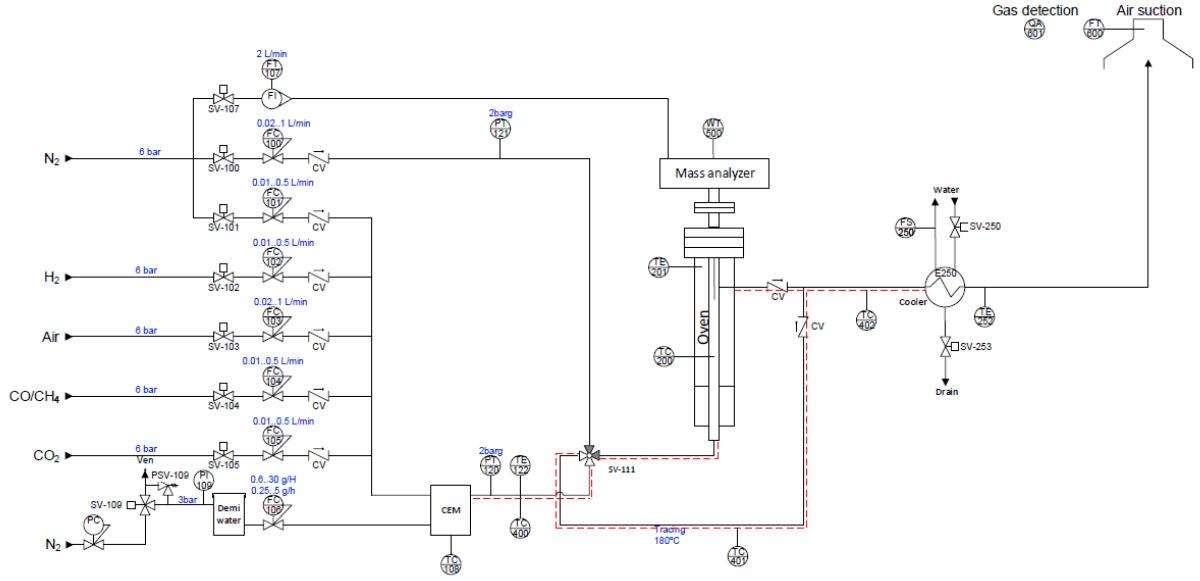

Figure 7: Setup for low pressure TGA, P&ID

The setup is composed by a quartz reactor inside an oven. The nitrogen line splits in three different lines: the first from the top is used for the mass analyzer, the second line is used when an inert atmosphere is required , whereas the third line is used when it is required as a carrier for other gases. All other reactive gases are connected to a C.E.M., which is used in case water vapor is needed. For this study, only N_2 and CO_2 are used.

The TGA setup was used in order to study: 1) the hydrophilicity of the membrane and 2) the surface adsorption of CO_2.

In order to study the hydrophilicity of the membrane, the carbon powder sample was hydrated in a climate chamber at a temperature of 20 ^{0}C and a humidity of 90% for three days. Then, 50 mg of the sample were analyzed in the TGA setup, according to the method shown in Figure 8: the sample is heated up to 400 °C with a heating rate of 5 °C while flushing 50 mL/min of nitrogen. Since N_2 is not expected to adsorb on the carbon membrane surface, each weight variation can be attributed to the water desorption. The maximum temperature (400 °C) was held for 1h more, in order to check for the weight stabilization.

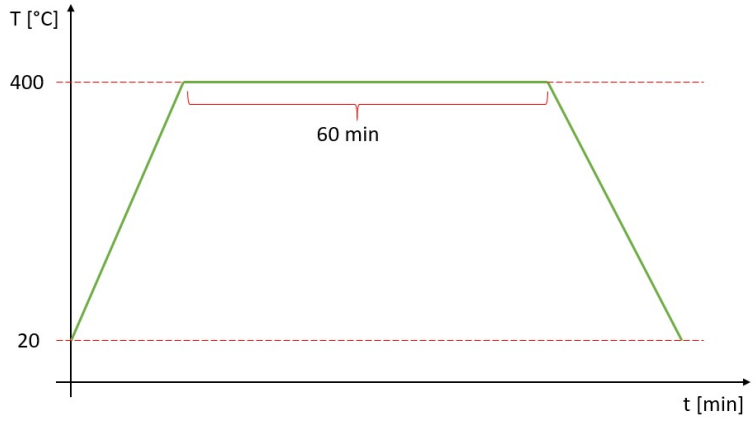

Figure 8: TGA water desorption schematic method

In order to study the CO_2 adsorption, a different procedure was adopted, whose schematic representation is shown in Figure 9**:** 50 mg of the sample were heated up to 200°C with a heating rate of 5°C while flushing 50 mL/min of nitrogen. Then, 200 mL/min of CO_2 were fed for 2h, recording the weight variation. An increase in the sample weight can be attributed to the adsorption of CO_2 on the carbon surface.

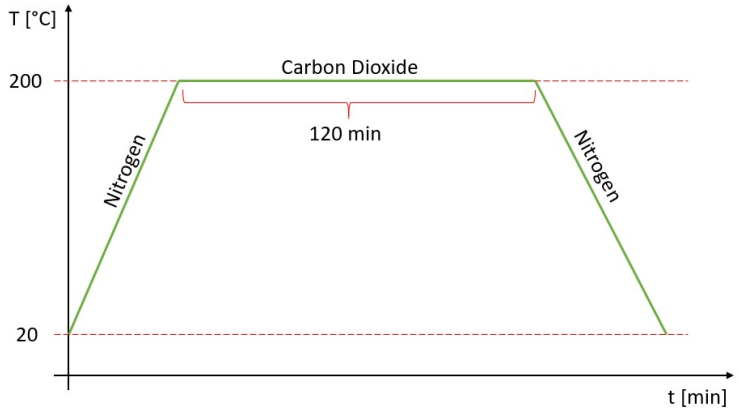

Figure 9: TGA CO_2 adsorption schematic method

The CO_2 adsorption was studied at 200 °C, which is in the middle of the temperature range used for the permeation experiments. The CO_2 adsorption was not studied systematically, because of the TGA setup limitation: only atmospheric pressure analysis was possible. Therefore, this analysis was performed only to understand if surface adsorption plays any role in the CO_2 permeation mechanism. The H_2 and CO adsorption was not studied, since it is expected that H_2 won't interact with the membrane surface, as it is a non-polar molecule, and CO bottle was empty at the time of the experiments.

3. Permeation setup

The setup used to perform vapor/gas permeation experiments is represented in Figure 10.

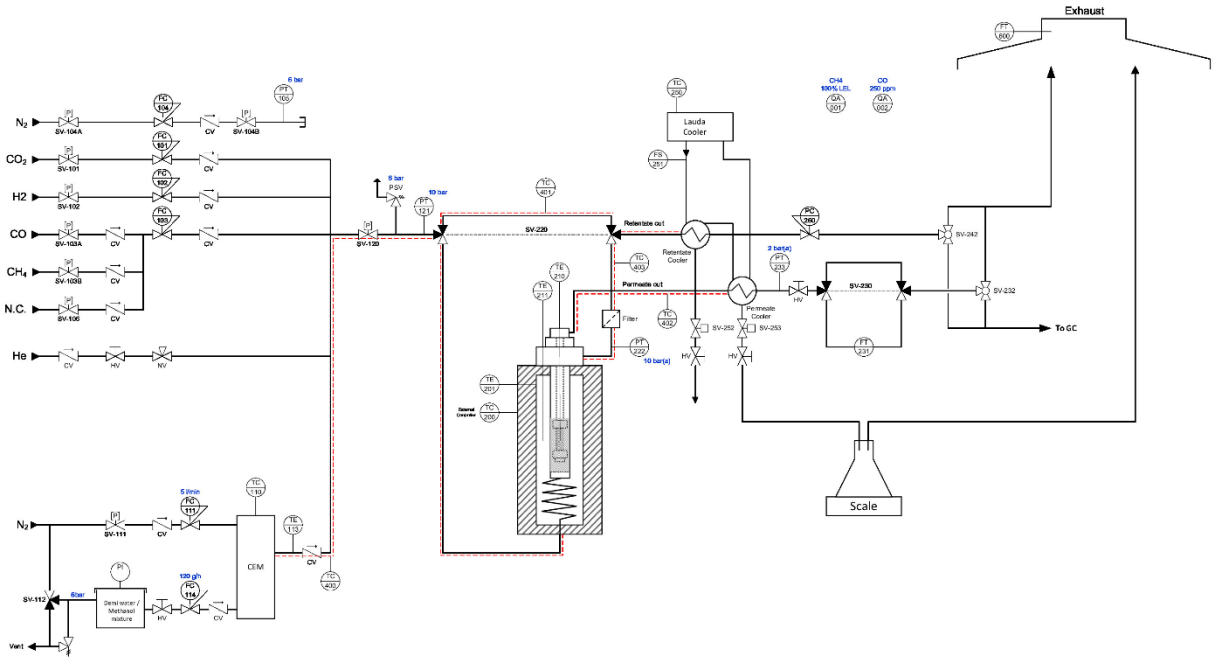

Figure 10: Vapor permeation setup, P&ID

This setup can be divided in four main sections: the feed section, the reactor section, the cooling section and the analysis section.

In the first section, the gas of interest and the vapor feed are present. In the upper section the gases are connected to the membrane reactor and controlled via flowmeters, which were previously calibrated. For this study, the gases of interest were N_2, H_2, CO_2 and CO. The liquid stream, water or methanol, was fed via the pressurized tank showed in the bottom. To vaporize the liquid flow, the line is connected to a Controlled Evaporator Mixer (C.E.M.) which operates in a range of 120-180°C. In order push the desired amount of liquid to the C.E.M. system and to pressurize the tank, a minimum nitrogen flowrate of 0.15L/min was required. To assure that liquid do not condense in the tubes, tracers are placed along the lines and operating at temperature between 170-220°C.

The membrane reactor consists of a stainless-steel vessel where the membrane is placed by connecting it through the top flange. The feed enters the reactor from the bottom, while permeate and retentate flows exit the reactor from its top part. The reactor is placed inside an electrical oven in order to assure isothermal conditions. Two thermocouples are used to control the temperature: one controls the bulk temperature and the second one is placed on the membrane surface.

After permeate and retentate exit the reactor, they pass through the cooling section for water removal. The cooling system is provided by Lauda. The water is liquified and collected into glass bottles, to be weighted. The gas streams are then sent to the analysis section. The permeate gas stream is connected to a bubble flowmeter and then to vent, whereas the retentate gas stream is connected to the μ-GC to study the gas composition, when required.

4. Vapor permeation tests

Vapor permeation test were performed to study the permeation of pure water and pure methanol. From these studies, also ideal selectivity of the system was derived. The ideal selectivity of a membrane does not consider the interactions between the compounds, as it is the ratio between the permeance of pure water and pure methanol systems, measured in the same conditions.

All the tests were conducted in the temperature range 150-250°C. The methodology used for permeation tests was the same for both water and methanol permeation test. The pressurized tank was filled with demi-water or pure liquid methanol. The retentate and permeate pressure was set to 4 and 1 bar, respectively, so that the pressure gradient acting on the membrane was constantly kept to 3 bar. Before starting each experiment, the N_2 flux through the membrane was measured. This was done to assure that the membrane was at comparable humidity condition before each vapor permeation test and that no aging had occurred.

Then, a total flowrate of 2 L^{vap}/min of water was fed to the membrane reactor, whereas for methanol permeation tests the total flowrate was 1.192 L^{vap}/min due to setup limitation. Specifically, it was not possible to feed more than 120 g/h of liquid through the C.E.M., which is less than the required amount to feed 2 L/min of methanol vapor. A minimum of N_2 gas flow was required to allow a correct operation of the C.E.M. However, the nitrogen volume fraction was chosen as low as possible, in order to assume a negligible effect on the vapor permeance. It is noteworthy to highlight that in both cases, the permeance was measured at steady state conditions.

The inlet conditions for both water and methanol permeation tests are summarized in Table 1 and Table 2:

Table 1: Inlet feed composition for water permeation test

	Vapor	Nitrogen
Flowrate	1.850 L/min	0.150 L/min
%vol	92.5	7.5

Table 2: Inlet feed composition for methanol permeation test

	Methanol	Nitrogen
Flowrate	1.042 L/min	0.150 L/min
%vol	87.5	12.5

The feed was continuously fed for 2 hours and the permeate and the retentate was then collected and measured. It has been demonstrated that at this point, the system is in steady state. A more detailed discussion on this can be found in Appendix B.

The permeance was computed as follow:

$$\wp\left[\frac{mol}{Pa\,m^2\,s}\right] = \frac{m\,[g]}{\Delta t\,[min]} * \left(\Delta P[Pa] * A_m[m^2] * 60[S] * MW_i\left[\frac{g}{mol}\right]\right)^{-1} \qquad Eq.\ 10$$

Where $\wp$ is the permeance of the specie, m the mass of permeate, Δt the experiment time span, ΔP the driving force acting on the membrane, A_m the estimated membrane area and MW_i the molecular weight of the specie.

The experiments were conducted for both membranes at operating temperature of 150°C, 200°C and 250°C, which is the application range desired for DME synthesis via membrane reactor.

After all the results were gathered, the ideal selectivity of the membrane was also calculated, as follows:

$$S_{MeOH} = \frac{\wp_{H_2O}}{\wp_{MeOH}} \qquad Eq.\ 11$$

where S_{MeOH} is the selectivity towards methanol, $\wp_{H2O}$ is the water permeance and $\wp_{MeOH}$ is the methanol permeance.

The only difference for ideal selectivity calculation is for the membrane carbonized at 700°C for the 250°C tests. Since the experimental data available were the one at 270°C, a fitting of the experimental data was done in order to calculate the permeance at 250°C. Detailed procedure is explained in Appendix A. The reason why initially the tests were performed at 270°C was to investigate methanol behaviour above its critical point. However, since the membrane sealing was leaking, a polymeric resin was used to fix it. Such resin is thermally unstable for temperature higher than 250°C. Thus, the following experiments were conducted at 250°C

5. H_2O/Gas mixtures

To study the real selectivity of H_2O/Gas, equimolar mixtures of water vapor and each gas were fed into the reactor. The total flowrate was set to 2L/min and the experiment time was set to 2 hours. The operating conditions were the same as the previous experiments. The gases that were studied in this section are: H_2, CO_2, CO.

Table 3: Inlet feed composition

	Water	Nitrogen	H_2 or CO_2 or CO
Flowrate	900 mL/min	200 mL/min	900 mL/min
%vol	45	10	45

The water was separated via condensation from both the permeate and the retentate, and weighted after 2 hours. The permeate gas flowrate was measured with a bubble flowmeter, while the retentate flow was sent to a μ-GC for the composition analysis. These information were sufficient to derive all the streams flow rate and composition, by solving mole balances on the species involved. Detailed calculations are reported in Appendix A.

Once that the permeate flowrate of the desired gas was computed, it was possible to calculate both water and gas permeance:

$$\wp_i = \frac{\Phi_i}{\Delta P_{ML,i} * A_m} \quad \text{or} \quad \wp_{H_2O} = \frac{\Phi_{H_2O}}{\Delta P_{ML,H_2O} * A_m} \qquad \textit{Eq. 12}$$

where ΔP_{ML} represents the logarithmic mean pressure gradient between permeate and retentate side. This value is different for water and gas, because it depends on the partial pressure of the considered compound.

$$\Delta P_{ML,i} = \frac{\Delta P_i^{in} - \Delta P_i^{out}}{ln\frac{\Delta P_i^{in}}{\Delta P_i^{out}}} \quad \text{or} \quad \Delta P_{ML,H_2O} = \frac{\Delta P_{H_2O}^{in} - \Delta P_{H_2O}^{out}}{ln\frac{\Delta P_{H_2O}^{in}}{\Delta P_{iH_2O}^{out}}} \qquad \textit{Eq. 13}$$

Knowing the permeance of both water and the desired gas, it is possible to calculate the selectivity as a ratio of the water permeance and the desired gas permeance, similarly to *Eq. 11.*

6. Model description

For this study, a phenomenological membrane reactor model was used for both the direct process and the first step of the indirect process (i.e. methanol production). The aim of these simulations is to compare the membrane reactor performance with a conventional reactor with no in situ water removal. The membrane properties used within the reactor model are the ones experimentally derived for both membrane samples.

6.1. Membrane reactor simulation for DME synthesis application

The model used for the process simulation represent a fixed bed membrane reactor composed by two coaxial tubes: the outer tube is the reactor shell, where the catalyst bed is inserted, and the inner tube represents the membrane. The water permeates from outer zone, which is the reaction zone, through the inner tube and reaches the permeation zone. This configuration is preferred due to a better mechanical stability of the membrane. A schematic representation of the membrane reactor is depicted in Figure 11.

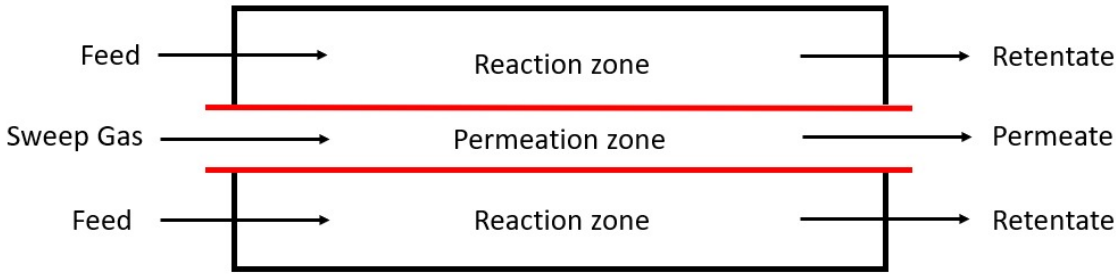

Figure 11: Schematic representation of the membrane reactor

To drive the permeation, a sweep gas is circulated in cocurrent mode. The sweep gas allows to keep the water partial pressure in the permeate side sufficiently low to assure a high driving force for its permeation. This is also the reason why a cocurrent configuration was chosen, as it is expected that most of the water will be produced close to the reactor inlet. Therefore, a higher driving force is required for water removal. Nonetheless, when using a sweep gas composition equal to the feed composition, the permeation of reactants through the membrane is lower, leading to a reduction in the loss of reactants

The hypotheses on which the membrane reactor model relies on are:

- Ideal plug flow;
- Steady state;
- Isothermal reactor;
- No pressure drops;
- Solid-gas phase are modeled as a single phase;
- Catalyst deactivation is neglected, as the operating temperature is low enough to avoid coke formation;
- The membrane material is considered inert.
- *For indirect process only*: it is assumed that the limiting step in the indirect process is the methanol production, therefore, only the first step is modeled and it is assumed that 85% methanol to DME conversion can be reached in the second step with a ractor temperature of 250°C. [37]

Mass balances are defined for each species for both the reaction and permeation zone (*Eq. 14* and *15*, respectively).

$$\frac{dF_i^R}{dz} = \rho_c(1-\varepsilon)\sum_{j=1}^{N_r}\left(r_j \nu_{ji}\right)\frac{\pi}{4}\left(D_{si}^2 - D_{mo}^2\right) - J_i \pi D_{mo} \qquad \textit{Eq. 14}$$

$$\frac{dF_i^P}{dz} = J_i \pi D_{mo} \qquad \textit{Eq. 15}$$

where J_i is the membrane flux for each species, defined as:

$$J_i = \wp_i \cdot \left(P_i^R - P_i^P\right) \qquad \textit{Eq. 16}$$

Where $\wp_i$ is the permeance of each component and $P^R{}_i$ and $P^P{}_i$ its partial pressure in the reaction or permeation zone respectively. According to the membrane flux definition in *Eq. 16*, it is positive when the compound permeates from the reaction to the permeation zone.

For the direct model, the kinetic model used to derive the reaction rates is the one developed by Lu et al. [40] for a $CuZnOAl_2O_3$/HZSM-5 bifunctional catalyst, which follows a Langmuir-Hinshelwood mechanism. [40], [41] The reaction rates derived from the kinetic model are the following:

$$r_1 = k_1 \frac{P_{CO_2} P_{H_2}\left(1 - \frac{1}{K_{p,1}} \frac{P_{H_2O} P_{CH_3OH}}{P_{CO_2} {P_{H_2}}^3}\right)}{\left(1 + K_{CO_2} P_{CO_2} + K_{CO} P_{CO} + \sqrt{K_{H_2} P_{H_2}}\right)^3} \qquad \textit{Eq. 17}$$

$$r_2 = k_2 \frac{\frac{1}{K_{p,2}} \frac{P_{CO_2} P_{H_2}}{P_{CO}} - P_{H_2O}}{\left(1 + K_{CO_2} P_{CO_2} + K_{CO} P_{CO} + \sqrt{K_{H_2} P_{H_2}}\right)} \qquad \textit{Eq. 18}$$

$$r_3 = k_3 \left(\frac{{P_{CH_3OH}}^2}{P_{H_2O}} - \frac{P_{CH_3OCH_3}}{K_{p,3}}\right) \qquad \textit{Eq. 19}$$

Where P_i is the partial pressure of each species. The kinetic, adsorption and equilibrium constants expression are listed below:

- Kinetic constants [40]:

$$k_1 = 35.45\ exp\left(-\frac{1.7609 \cdot 10^4}{RT}\right) \qquad \frac{kmol}{(kg_{cat} \cdot s \cdot bar^2)} \qquad \textit{Eq. 20}$$

$$k_2 = 7.3976\ exp\left(-\frac{2.0436 \cdot 10^4}{RT}\right) \qquad \frac{kmol}{(kg_{cat} \cdot s \cdot bar)} \qquad \textit{Eq. 21}$$

$$k_3 = 8.2894 \cdot 10^4\ exp\left(-\frac{5.2940 \cdot 10^4}{RT}\right) \qquad \frac{kmol}{(kg_{cat} \cdot s \cdot bar)} \qquad \textit{Eq. 22}$$

- Adsorption constants [42][49]:

$$K_{H_2} = 0.249\ exp\left(\frac{3.4394 \cdot 10^4}{RT}\right) \qquad \frac{1}{bar} \qquad \textit{Eq. 23}$$

$$K_{CO_2} = 1.02 \cdot 10^{-7}\ exp\left(\frac{6.74 \cdot 10^4}{RT}\right) \qquad \frac{1}{bar} \qquad \textit{Eq. 24}$$

$$K_{CO} = 7.99 \cdot 10^{-7}\ exp\left(\frac{5.81 \cdot 10^4}{RT}\right) \qquad \frac{1}{bar} \qquad \textit{Eq. 25}$$

- Equilibrium constants [43] [49]:

$$ln(K_{p,1}) = 4213/T - 5.752 \cdot ln(T) - 1.707 \cdot 10^{-3}T + 2.682 \cdot 10^{-6}T^2 + -7.232 \cdot 10^{-10}T^3 + 17.6 \qquad \textit{Eq. 26}$$

$$log(K_{p,2}) = 2167/T - 0.5194 \cdot log(T) + 1.037 \cdot 10^{-3}T - 2.331 \cdot 10^{-7}T^2 - 1.2777 \qquad \textit{Eq. 27}$$

$$ln(K_{p,3}) = 4019/T + 3.707 \cdot ln(T) - 2.783 \cdot 10^{-3}T + 3.8 \cdot 10^{-7}T^2 + -6.56 \cdot 10^4/T^3 - 26.64 \qquad \textit{Eq. 28}$$

The same reactor structure and design concept was used for modeling the first step of the indirect process for DME production. Compared to the direct model, the indirect model considers the same species, except for DME, which is not produced in the first reactor. The catalyst used for the kinetic study and reaction rates evaluation is $Cu/ZnO/Al_2O_3$. [44] The reactions on which the kinetic model for methanol production is based are:

$$CO + 2H_2 \rightleftarrows CH_3OH \qquad \Delta H_0 = -90.7\ kJ/mol \qquad \textit{Eq. 29}$$

$$CO_2 + H_2 \rightleftarrows CO + H_2O \qquad \Delta H_0 = +41.2\ kJ/mol \qquad \textit{Eq. 30}$$

$$CO_2 + 3H_2 \rightleftarrows CH_3OH + H_2O \qquad \Delta H_0 = -49.5\ kJ/mol \qquad \textit{Eq. 31}$$

Consequently, the reaction rates derived from the kinetic model are:

$$r_1 = k_1 K_{CO} \frac{P_{CO} P_{H_2}^{3/2} - \frac{P_{CH_3OH}}{K_{p,1} P_{H_2}^{\frac{1}{2}}}}{(1+K_{CO}P_{CO}+K_{CO_2}P_{CO_2})[P_{H_2}^{\frac{1}{2}} + \frac{K_{H_2O}}{K_{H_2}^{\frac{1}{2}}} P_{H_2O}]} \qquad \textit{Eq. 32}$$

$$r_2 = k_2 K_{CO_2} \frac{P_{CO_2} P_{H_2} - \frac{P_{CO} P_{H_2O}}{K_{p,2}}}{(1+K_{CO}P_{CO}+K_{CO_2}P_{CO_2})[P_{H_2}^{\frac{1}{2}} + \frac{K_{H_2O}}{K_{H_2}^{\frac{1}{2}}} P_{H_2O}]} \qquad \textit{Eq. 33}$$

$$r_3 = k_3 K_{CO_2} \frac{P_{CO_2} P_{H_2}^{3/2} - \frac{P_{CH_3OH} P_{H_2O}}{K_{p,3} P_{H_2}^{\frac{3}{2}}}}{(1+K_{CO}P_{CO}+K_{CO_2}P_{CO_2})[P_{H_2}^{\frac{1}{2}} + \frac{K_{H_2O}}{K_{H_2}^{\frac{1}{2}}} P_{H_2O}]} \qquad \textit{Eq. 34}$$

Where P_i is the partial pressure of each species. The kinetic, adsorption and equilibrium constants expression are listed below:

- Kinetic constants [44]:

$$k_1 = 4.89 \cdot 10^7 \, exp\left(-\frac{113000}{RT}\right) \quad \frac{mol}{(kg_{cat} \cdot s \cdot bar)} \qquad \textit{Eq. 35}$$

$$k_2 = 4.84 \cdot 10^{11} \, exp\left(-\frac{140454}{RT}\right) \quad \frac{kmol}{(kg_{cat} \cdot s \cdot bar^{1/2})} \qquad \textit{Eq. 36}$$

$$k_3 = 23.4 \, exp\left(-\frac{5.2940 \cdot 10^4}{RT}\right) \quad \frac{kmol}{(kg_{cat} \cdot s \cdot bar)} \qquad \textit{Eq. 37}$$

- Adsorption constants [45]:

$$K_{CO} = 2.16 \cdot 10^{-5} \, exp\left(\frac{46800}{RT}\right) \quad \frac{1}{bar} \qquad \textit{Eq. 38}$$

$$K_{CO_2} = 7.05 \cdot 10^{-7} \, exp\left(\frac{61700}{RT}\right) \quad \frac{1}{bar} \qquad \textit{Eq. 39}$$

$$\frac{K_{H_2O}}{K_{H_2}^{\frac{1}{2}}} = 6.37 \cdot 10^{-9} \, exp\left(\frac{84000}{RT}\right) \quad \frac{1}{bar^{1/2}} \qquad \textit{Eq. 40}$$

- Equilibrium constants [45]:

$$log(K_{p,1}) = \frac{5139}{T} - 12.621 \qquad \frac{1}{bar^2} \qquad \textit{Eq. 41}$$

$$log(K_{p,2}) = -\frac{2073}{T} + 2.0929 \qquad \textit{Eq. 42}$$

$$ln(K_{p,3}) = \frac{3066}{T} - 10.592 \qquad \frac{1}{bar^2} \qquad \textit{Eq. 43}$$

For both processes, the traditional thermodynamic limit for conventional reactor was calculated by using ASPEN Plus (V10) by means of a RGibbs reactor. This limit was used to compare the membrane reactor performance with the conventional reactor. The model was also validated, as reported in Appendix D.

Lastly, conversion and yield of the compounds are calculated, considering also the trans-membrane flux as:

$$X = \frac{F_{CO_2}^{in} - F_{CO_2} + F_{CO_2}^{tmb}}{F_{CO_2}^{in} + F_{CO_2}^{tmb}} \qquad \textit{Eq. 44}$$

$$Y_i = \frac{F_i^R + F_i^P}{F_{CO_2}^{in} + F_{CO_2}^{tmb}} \qquad \textit{Eq. 45}$$

Chapter 4
Results and discussion

1. Characterization

1.1. Pore size distribution

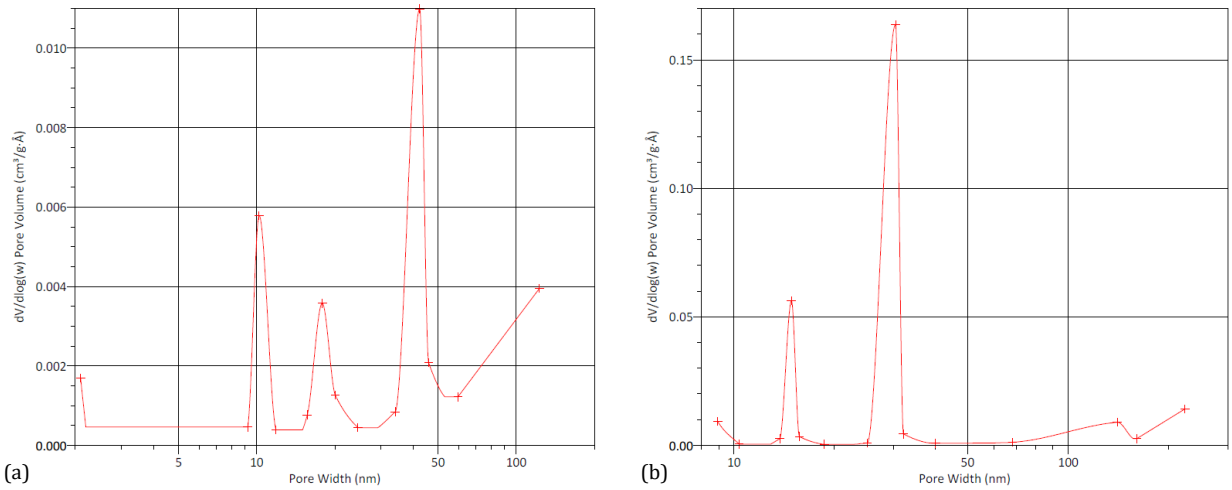

Figure 12: Pore size distribution of the carbon membrane carbonized at 600℃ (a) and 700℃ (b)

Figure 12a and Figure 12b show the pore size distribution of the membrane carbonized at 600°C and 700 °C, respectively. The membrane carbonized at 700°C shows a bimodal curve, which is typical for carbon membranes. However, a different behaviour is observed for the membrane carbonized at 600 °C, which shows three different peaks. Both the membranes show mainly mesopores, with the membrane carbonized at lower temperature having a mean pore size larger (42.44 nm) than the one carbonized at higher temperature (30.4 nm). This trend is typical for carbon membranes when increasing the carbonization temperature. When the carbon layer is treated at 700°C or higher, the amount of functional groups in the membrane structure decreases. This decrease causes a reduction of the interplanar spacing

between the carbon layers. Therefore a more dense and crystalline structure is obtained [18]. A smaller mean pore size generally leads to a decrease in the permeance and an increase in the selectivity.

However, both the graphs show that the lines tend to raise both at the beginning and at the end. The reason why the analysis is imprecise is because the desorption was not fully completed. The last detected desorption point was at relative pressure of 0.12 for both the samples The reason could be that the Nitrogen molecules are trapped in the carbon micropores and due to the low kinetic energy at 77K, the molecules cannot get out from the bottle shaped micropores.

To better evaluate the pore size distribution of the carbon membranes, it is advisable to use CO_2 instead of liquid nitrogen. The reason being that CO_2 adsorption analysis is usually conducted at 0°C, therefore the CO_2 molecules have higher kinetic energy to exit the micropores and desorbs from the membrane.

From these results, it is possible to qualitatively conclude that the measured mean pore size of both the membranes is in the mesopores range (50 to 2 nm). It is reasonable to think that micropores are also present, and their distribution might even be higher than mesopores, however it is not possible to detect them with the used apparatus.

In both cases, the transport should be surface diffusion coupled with Knudsen diffusion when only gas are considered. When condensable vapor is considered, capillary condensation may happen. However, in mesopores is not possible to have full condensation for this specific case. From Figure 13, it can be seen that in order to have full condensation, a higher capillary condensation pressure is needed in order for water to fully condensate into mesopores. This graph is built based on the Kelvin equation (*Eq.5*).

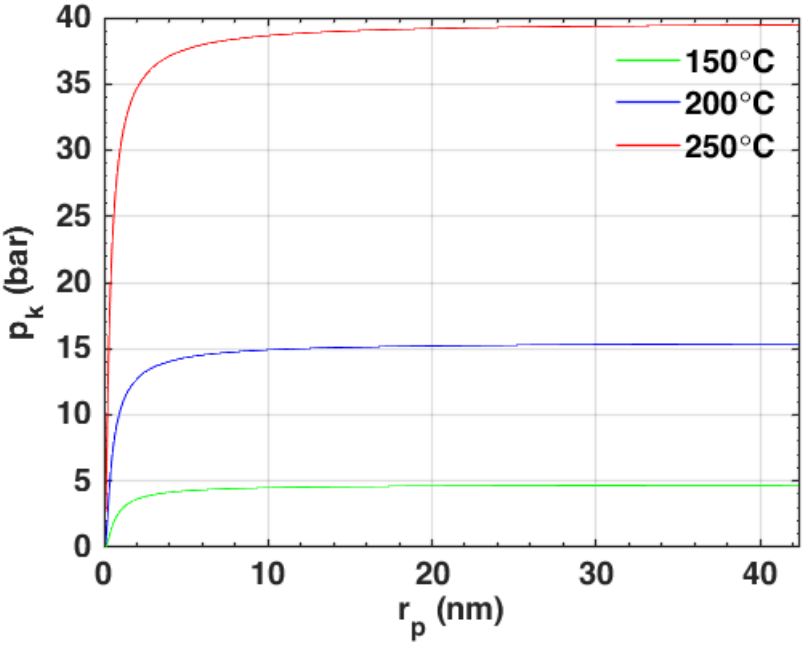

Figure 13: Description of capillary condensation dependency on mean pore radius and pressure depicted by Kelvin's equation at different operating temperatures.

However, as the detection of micropores and ultramicropores is limited by the equipment used, it is not possible to correctly draw conclusion on the transport mechanisms involved. Indeed, having a wide distribution of ultramicropores and micropores would make the molecular sieve mechanism the major transport contribution. Nonetheless, it is possible to suppose from what reported in Chapter 2 that this is the case.

1.2. Functional groups

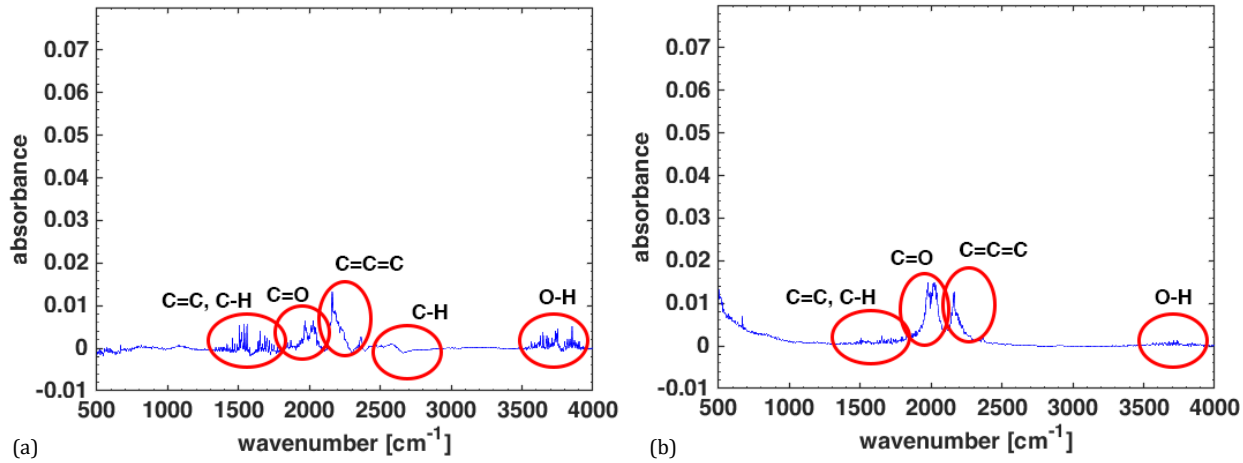

Figure 14: FTIR results for the membrane sample CM600 (a) and for the CM700 (b). They show the functional groups present on the carbon film after pyrolysis.

In Figure 14 the normalized results from the FTIR analysis are presented with peak identification for each spectrum. The normalization was done by correcting the base line so that the signal was normalized for the amount of sample. In Figure 14a, the spectrum of the membrane carbonized at 600°C generally shows a higher density of functional groups and a higher intensity signal. Therefore, the identification of the peaks was done on this spectrum.

Starting from the lower wavenumbers, between 1450 and 1600 cm^{-1}, CH bending and C=C stretching can be identified. Within 1650 and 2000 cm^{-1} C=O stretching signal are present, followed by C=C=C stretching. A weak signal of C-H stretching can be seen between 2695 and 2830 cm^{-1}. Lastly, between 3500 and 4000 cm^{-1} O-H stretching peaks are present. [50]

In the membrane sample CM600, a higher number of functional groups are present, especially OH groups, which may be responsible for the membrane hydrophilicity. The only different trend is the C=O peak, which is increased in the membrane carbonized at 700°C. This may be due to a rearrangement of the membrane morphology.

Thus, when increasing the carbonization temperature, the membrane surface is subject to changes, due to the functional groups decomposition. However, it is not possible to clearly define which membrane sample is more hydrophilic between the two with FTIR results only. Indeed, the increase in C=O functional groups in Figure 14b may also affect the membrane

sample hydrophilicity, as it is a polar functional group. Therefore, a TGA water desorption study was also implemented to determine which sample has higher water affinity.

1.3. TGA

1.3.1. Water desorption

The TGA analysis was conducted to investigate the water desorption from a fully hydrated membrane surface. The results are depicted in Figure 15a and Figure 15b for the membrane carbonized at 600 °C and 700 °C, respectively.

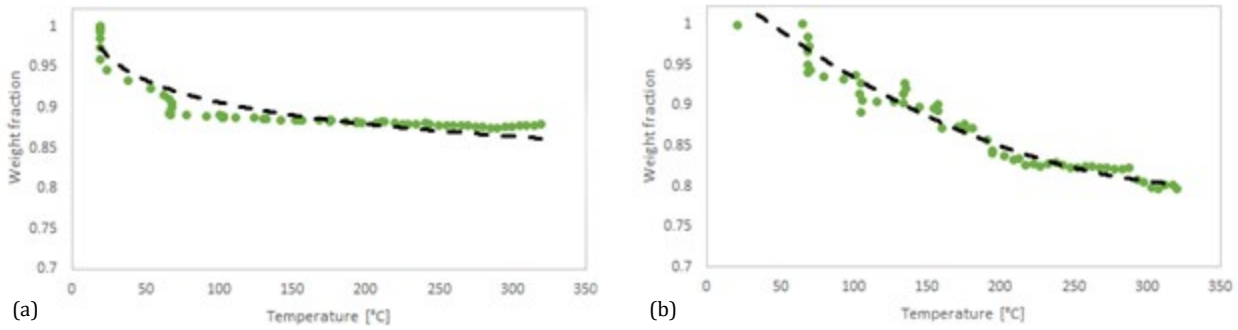

Figure 15: Weight loss of hydrated powder sample of the membrane sample CM600 (a) and the CM700 (b).

By comparing the two curves, the membrane carbonized at 600°C shows a faster water desorption with respect to the membrane carbonized at 700°C. The reason for that may rely on the membrane pore size: as the pores are wider for the membrane carbonized at 600°C, the water can evaporate and leave the membrane more easily at lower temperatures. However, it may also depend on a weaker water-surface interaction compared to CM700.

Indeed, the weight loss at the equilibrium is lower for the CM600 (86%) with respect to the CM700 (80%). This may be due to the initial amount of water that actually adsorbed on the membrane surface. As seen in Figure 14a and Figure14b, the C=O functional group signal increases with increase in carbonization temperature. This group is also polar, so may play a role in determine the membrane hydrophilicity, counterbalancing the effect of the -OH functional groups. Moreover, the water desorbs faster in the CM600 sample, therefore, its hydrophilic behavior should be weaker than the CM700 membrane sample.

In conclusion, the TGA results confirm that the carbon layer is hydrophilic, and water adsorbs on the membrane surface with stronger interactions when carbonization temperature is higher.

1.3.2. CO_2 adsorption

Figure 16 shows the results of the CO_2 adsorption for the membrane carbonized at 600 °C and 700 °C, respectively. The relevant information are present after around 60 minutes, as before a lot of noise, due to equipment instability and sensitivity, is present.

It is clear that CO_2 is adsorbed on the carbon layer of both the membranes, since the sample weight increases over time when exposed to a flow of CO_2. This proves that the carbon dioxide interacts with the functional groups of the carbon film. Moreover, it is possible to see that the CM700 has a slightly stronger interaction compared to the CM600, which may depend on the C=O polarity. Thus, a surface-diffusion type of mechanism is expected to play a role in the CO_2 permeation through the carbon membrane. When CO_2 adsorbs on the membrane surface, the actual pore size is reduced. Therefore, larger molecules, as CO, should permeate less easily through the pores.

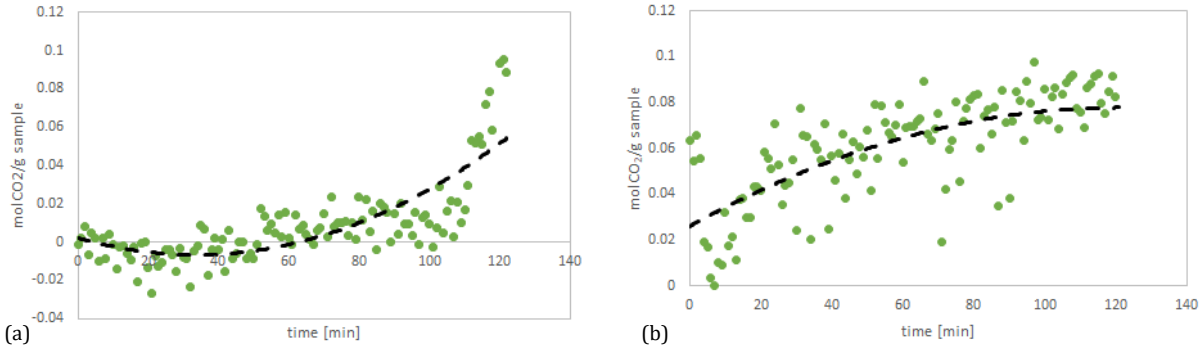

Figure 16: CO_2 adsorbed on the sample surface over time for CM600 (a) and CM700 (b)

2. Water permeation

The aim of this set of experiments is to understand how the membrane permeance is influenced by the operating temperature, the carbonization temperature and which transport mechanism prevails during the permeation. The prevailing transport mechanism is difficult to quantitively estimate. However, it is possible to make qualitative hypothesis from the experimental data gathered at the end of this stage.

Figure 17 shows the water permeance as a function of the operating temperature for the membranes carbonized at 600 °C and 700 °C. Values are also reported in Table 4. The first observation is that both the membranes show comparable water permeance values, and their difference is within the experimental error. Water permeance is clearly decreasing when increasing temperature, indicating that an exothermic transport mechanism is predominant. Such trend can be justified by both the capillary condensation phenomenon and the surface diffusion transport mechanism.

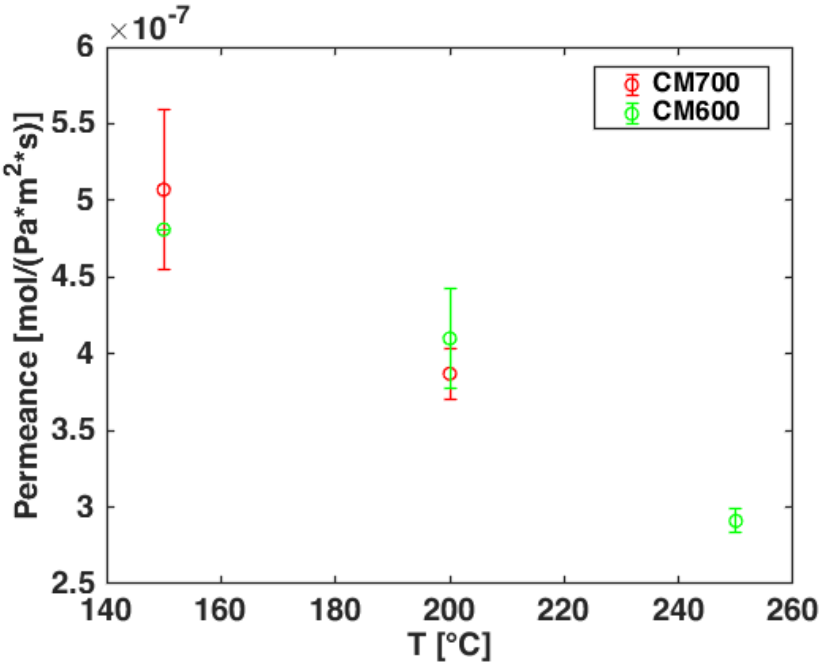

Figure 17: Water vapor permeance of CM600 and CM700 membrane samples. The permeance plotted is the average value of the results obtained by each test. The error bar shows the standard deviation from the avegare value.

Table 4: Water vapor permeance of CM600 and CM700 membrane samples.

Membrane sample	Permeance at T=150°C [mol/Pa/m^2/s]	Permeance at T= 200°C [mol/Pa/m^2/s]	Permeance at T=250°C [mol/Pa/m^2/s]
CM700	$5.07 \cdot 10^{-7} \pm 5.23 \cdot 10^{-8}$	$3.87 \cdot 10^{-7} \pm 1.63 \cdot 10^{-8}$	$2.91 \cdot 10^{-7} \pm 7.78 \cdot 10^{-9}$
CM600	$4.81 \cdot 10^{-7} \pm 0$	$4.10 \cdot 10^{-7} \pm 3.25 \cdot 10^{-8}$	$2.91 \cdot 10^{-7} \pm 7.78 \cdot 10^{-9}$

The similar permeance is given by a counterbalance of two different effects. From BET results, it is known that the membrane at higher carbonization temperature has smaller pores. Therefore, the permeance should decrease with increase in carbonization temperature. However, since capillary condensation is also related to the pore radius by the Kelvin's equation (*Eq. 5*), this can affect the water permeance. Indeed, a decrease of the pore size leads to a decrease in saturation pressure of water, which can condense more easily in the smaller pores. Moreover, this effect is enhanced by the higher hydrophilic behavior of the CM700 membrane, which overall increase the water flux through the membrane.

Thus, two mechanisms are controlling the water permeance: capillary condensation, which mainly depends on pore size distribution, and surface diffusion on functional groups. The combination of these two effects leads to a compensation, which results in similar

permeances. Water permeance is decreasing when increasing the operating temperature, for both the membranes. This trend is expected when condensation plays a role in the water permeation mechanism. Water is fed in the membrane reactor as superheated vapor (at 4 bar, water boiling point is 143.63°C). As soon as water enters the pores, condensation temperature increases (see Kelvin' s equation) and the permeation is enhanced. Therefore, it is reasonable to say that the lowest the operating temperature, the closest to the condensation the vapor is, the easiest is for water to condensate when entering the pores. Thus, the amount of liquid within the membrane should be higher, as the water flux through the membrane and, therefore, the permeance.

This behavior is also confirmed by the analysis of the activation energy of the permeation, which correlate the permeation as a function of the temperature. This relationship is shown in the ln(P) vs 1/T graph in Figure 18.

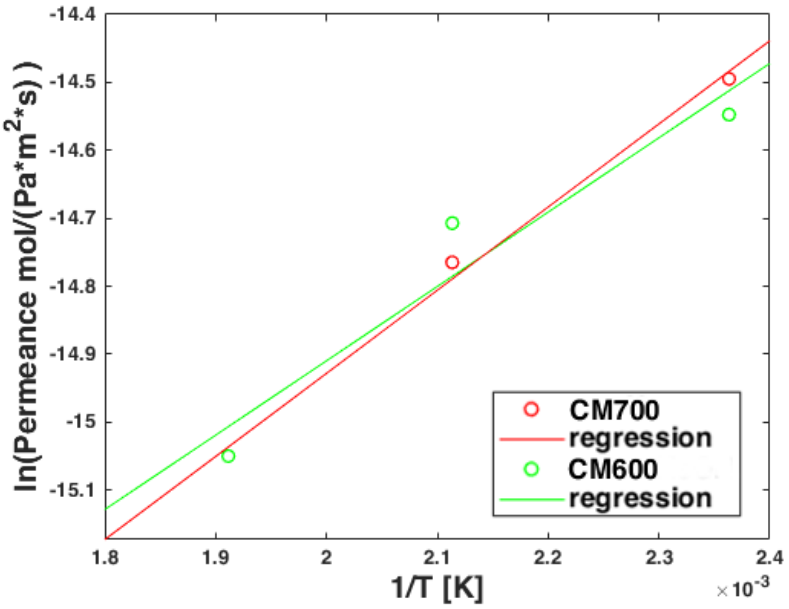

Figure 18: Activation energy of permeation for both membrane samples. The fitting of the data point is made by linear regression. Details of the calculation are reported in Appendix C.

Assuming that the permeance follows an Arrhenius like relationship, then it can be correlated to the activation energy via the following equation:

$$\wp = \wp_0 \, exp\left(-\frac{E_a}{RT}\right) \qquad \textit{Eq. 46}$$

where $\wp$ is the permeance, $\wp_0$ is the permeance at $1/T$=0, E_a the activation energy, R the ideal gas constant and T the operating temperature. The activation energy can be expressed as the product of diffusion and adsorption energy, resulting in E_a being the sum of the diffusion energy and the sorption energy. The diffusion energy is usually positive, whereas the

sorption energy may be negative. [46] When the adsorption energy overcomes the diffusion one, then the overall activation energy of the permeation become negative. Thus, the permeance decreases with operating temperature.

Table 5: Activation energy of permeation and $\wp_0$ values for the CM600 and CM700 membranes

Membrane sample	$\wp_0$ at $1/T = 0$ [mol/Pa/m^2/s]	Activation Energy [J/mol]
CM700	$2.828 \cdot 10^{-8}$	-10193.79
CM600	$3.746 \cdot 10^{-8}$	-9102.17

When carbon membranes are compared to zeolites, the water permeance in carbon membranes is higher than the minimum value reported by Diban et al. [20], which is based on literature review of zeolite membranes performances. Thus, carbon membranes show competitive water permeance and, in some cases, can perform better than zeolite membranes, becoming a promising alternative.

3. Methanol permeation

Methanol permeation experiments were performed in order to investigate the membrane perm-selectivity between water and methanol. This parameter is a key factor in the membrane selection for the DME synthesis process. If the membrane shows low methanol permeance (i.e., high water to methanol selectivity), it is a suitable candidate for the direct route application, otherwise the indirect route should be considered.

Methanol permeance was measured at the same operating conditions of the water vapor permeation test for both the membranes. The results are presented in Figure 19:

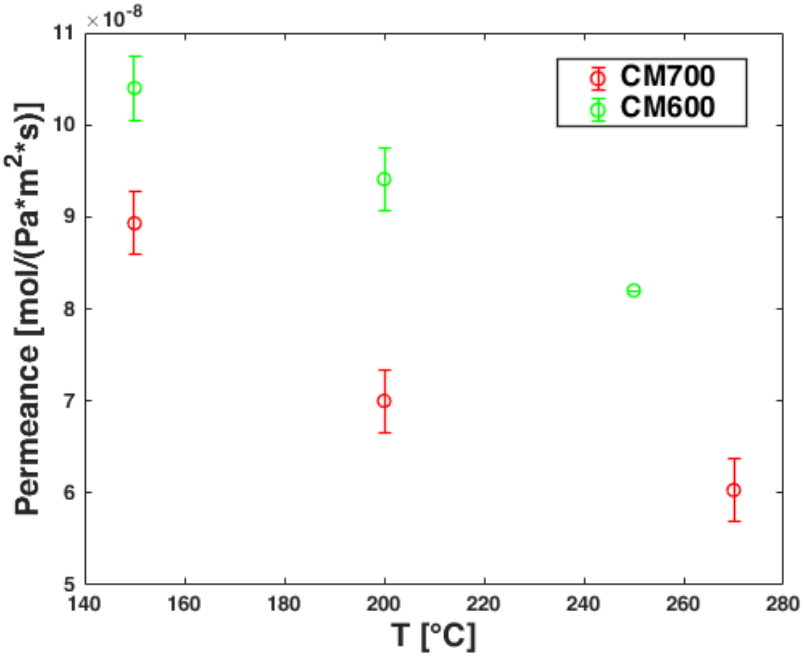

Figure 19: Methanol mean permeance of CM700 and CM600 membrane samples. The permeance plotted is the mean value of the results obtained from each test. The error bar shows the standard deviation from the mean value.

Table 6: Experimental evaluation of methanol mean permeance at different operating temperatures.

Membrane sample	Permeance at T=150°C [mol/Pa/m²/s]	Permeance at T=200°C [mol/Pa/m²/s]	Permeance at T=250°C [mol/Pa/m²/s]
CM700	$8.93 \cdot 10^{-8} \pm 3.39 \cdot 10^{-9}$	$7.00 \cdot 10^{-8} \pm 3.39 \cdot 10^{-9}$	$6.33 \cdot 10^{-8} \pm 3.39 \cdot 10^{-9}$
CM600	$1.04 \cdot 10^{-7} \pm 3.54 \cdot 10^{-9}$	$9.41 \cdot 10^{-8} \pm 3.39 \cdot 10^{-9}$	$8.20 \cdot 10^{-8} \pm 0$

Similarly to water permeation tests, the methanol permeance decreases when increasing temperature, suggesting that surface-diffusion is affecting also the methanol flux through the membrane. However, there is an appreciable difference between the permeances of the two membranes. This is due to the weaker adsorption of methanol on the membrane surface and the absence of capillary condensation. Since methanol molecules are less polar than water molecule, it is likely that their adsorption on the membrane surface is weaker. Moreover, since the operating conditions are far from the saturation conditions of methanol, capillary condensation is unlikely to happen. Therefore, methanol permeation depends both on the pore size of the membrane, as there is no "pore blocking" effect due to capillary condensation, and on the surface diffusion of methanol through the membrane. Indeed, the contribution of

the surface-diffusion mechanism is confirmed by the tendency of the permeation to decrease with increase in operating temperature.

Furthermore, in this case the influence on the permeance of smaller pore size is relevant, as MeOH only weakly interact with the membrane surface. This may enforce the discussion on the water permeance results reported in the previous section.

Another aspect that was investigated was the effect of methanol critical temperature. Indeed, the critical temperature of methanol is 240.2°C, which is in the experimental range of the operating temperature used in this study. However, no relevant difference in the permeance behavior was observed when the membrane operates above the critical temperature. It is possible that more appreciable difference may be observed if the operating temperature is far enough from the critical one.

4. Water/Methanol ideal perm-selectivity

Although the membrane carbonized at 600°C and 700°C show comparable water permeance, the difference in methanol permeance will affect their ideal perm-selectivity. The ideal perm-selectivity for this system is defined as the ratio of the water permeance and the methanol permeance, when they are derived in pure system:

$$S_{MeOH} = \frac{\wp_{H_2O}}{\wp_{MeOH}} \qquad \text{Eq. 47}$$

where the permeance used are the ones evaluated experimentally in Section 2 and Section 3.

The ideal case would be a membrane with high water permeance and high selectivity, so that the methanol loss would be kept at minimum. However, a well-established trend shows that selectivity decreases when permeance increases and vice versa [47],[48]. These membranes show good water/methanol perm-selectivity, considering that the two molecules show similar behavior (i.e., polarity, possibility to condense within the pores). Moreover, the difference in perm-selectivity between the two membranes is relatively small, as can be seen in Figure 20 .

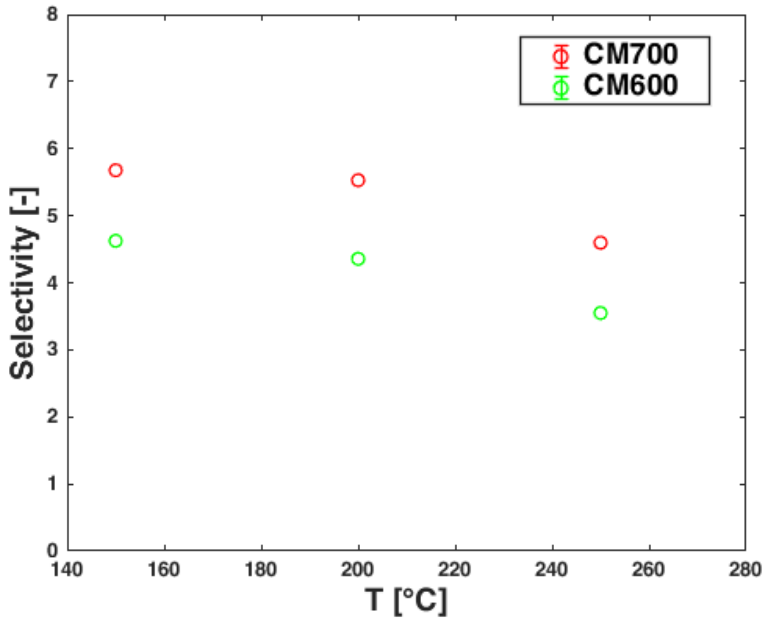

Figure 20: Ideal selectivity vapor/methanol system of the membrane samples. The higher selectivity of the 405-N is expected as it has a lower methanol permeance.

Table 7: Ideal selectivity values evaluated from experimental data.

Membrane sample	S_{MeOH} [T=150°C]	S_{MeOH} [T=200°C]	S_{MeOH} [T=250°C]
CM700	5.678	5.529	4.598
CM600	4.625	4.357	3.549

The ideal perm-selectivity of both membranes are higher compared to zeolite membranes found in literature, which have a maximum of 2.8, showing that carbon membranes have better separation properties. [20] Thus, as higher selectivity is needed, carbon membranes might be a better choice for direct process application. The ideal selectivity of the membrane carbonized at 700°C is slightly higher compared to the 600°C. This is in line with the methanol permeation results, which adsorbs less on the membrane carbonized at higher temperature.

A drawback of ideal selectivity, however, is that it does not consider the interaction between water and methanol molecules when mixed. A more precise analysis would consider the real selectivity of the mixture. However, because of some setup limitations, it was not possible to test the membranes in these conditions.

In conclusion, the membrane CM700 should be a more suitable choice for DME production. This assumption will be confirmed using the phenomenological membrane reactor model described in the previous Chapter.

5. Real selectivity for H_2O/Gas mixtures

Lastly, real selectivity for water/gas mixtures were evaluated. Real selectivity in this case is preferred over ideal selectivity for two reason. The first being that real selectivity of a mixture considers the chemical interaction between molecules, other than the interaction between the single species and the membrane. The second reason is because of the hydrophilicity of carbon membranes. As already mentioned in Chapter 1, carbon membranes show hydrophilic behavior that is often considered a drawback in gas separation. Indeed, when water is adsorbed on the membrane surface, a change of gas diffusivity through the membrane occurs. Moreover, when capillary condensation occurs, the actual membrane pore size is smaller, and the gases permeation is inhibited. In this study, this "pore-blocking" effect is desired, since the ideal scenario is when water, alone, permeates through the membrane, leaving the gases available for further reaction on the catalytic bed.

Figure 21 shows the real selectivity for H_2O/H_2, H_2O/CO_2 and H_2O/CO derived from equimolar mixture.

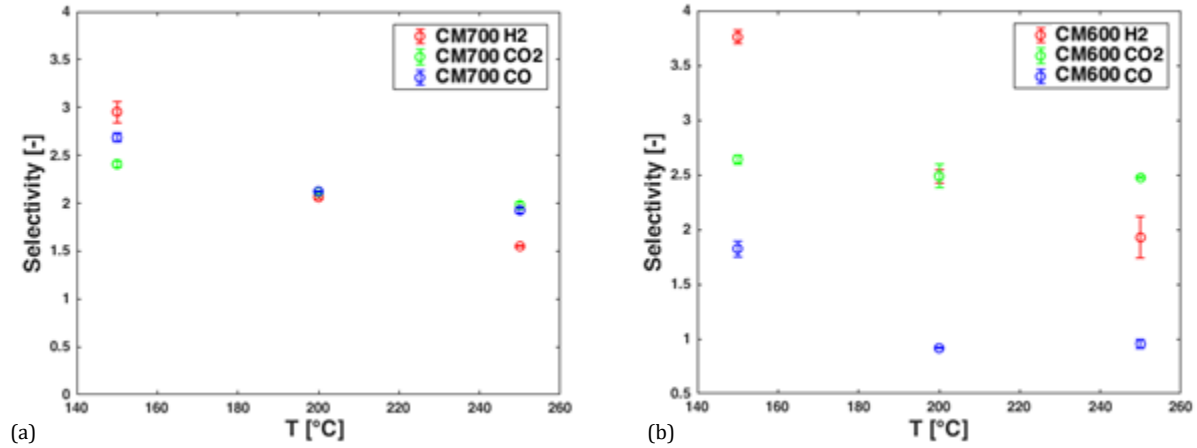

Figure 21: Real selectivity of H_2O/H_2, H_2O/CO_2 and H_2O/CO mixtures for CM700 (a) and CM600 (b).

The water/gas separation depends on several parameters, which are related to the predominant transport mechanism. When molecular sieving or Knudsen diffusion is predominant, the separation depends on the kinetic diameter of the molecules. Moreover, if water condenses in the pores, two phenomena must be considered: 1) gas molecules can

solubilize in the condensed water and the selectivity depends on the solubility of the gas in water and 2) the pore-blocking effect reduces the pore size and the selectivity depends again on the gas molecule size. In Table 8 the kinetic diameter and the solubility of the molecules of interest are summarized.

Table 8: Kinetic diameter and solubility in water of hydrogen, carbon dioxide and carbon monoxide

	Kinetic diameter [Å]	Solubility at 20°C [$g_{gas}/100g_{H2O}$]
H_2O	2.65	-
H_2	2.89	0.00016
CO_2	3.3	0.169
CO	3.76	0.0028

As hydrogen is the less soluble in water, it is believed that the contribution of its solubility to the permeation is negligible. Therefore, the highest selectivity of H_2 at the lowest operating temperature is due to the "pore-blocking" effect of water. As the effect of capillary condensation decreases when increasing temperature, hydrogen can pass through the pores easily, due to a lower pore-blocking effect.

The hydrogen selectivity is higher for the membrane at lower carbonization temperature, although the pores are wider. This might be due to a higher capillary condensation, so it is likely that its clogging effect is more prominent compared to the other sample. Indeed, water permeance is higher for the membrane carbonized at 600°C, whereas the hydrogen permeance is comparable between the two samples. Therefore, hydrogen permeates less easily in CM600 rather than CM700. Details about the experimental values of all the gas and water permeances are reported in Appendix A, Section 4.

The water permeance slightly decreases with increasing temperature, suggesting that capillary condensation still plays an important role in the permeation mechanism. In Figure 22, the water permeance in single vapor experiment is compared to the water permeance for vapor/gas mixtures[1]. It is possible to notice that the water permeance values decrease compared to single vapor system. This is due to the decrease of the partial pressure of water in the mixture system. Moreover, the decrease of permeance with temperature for water in the mixture is less predominant than in single system. This suggest that, although capillary

[1] This is just one example, considering H_2O/CO_2 mixture. The trend is the same for all the mixtures and this can be further confirmed in Appendix A, Section 4

condensation still plays a role, it is not as predominant as it was for single vapor permeance experiments, which also depends on the decrease in partial pressure.

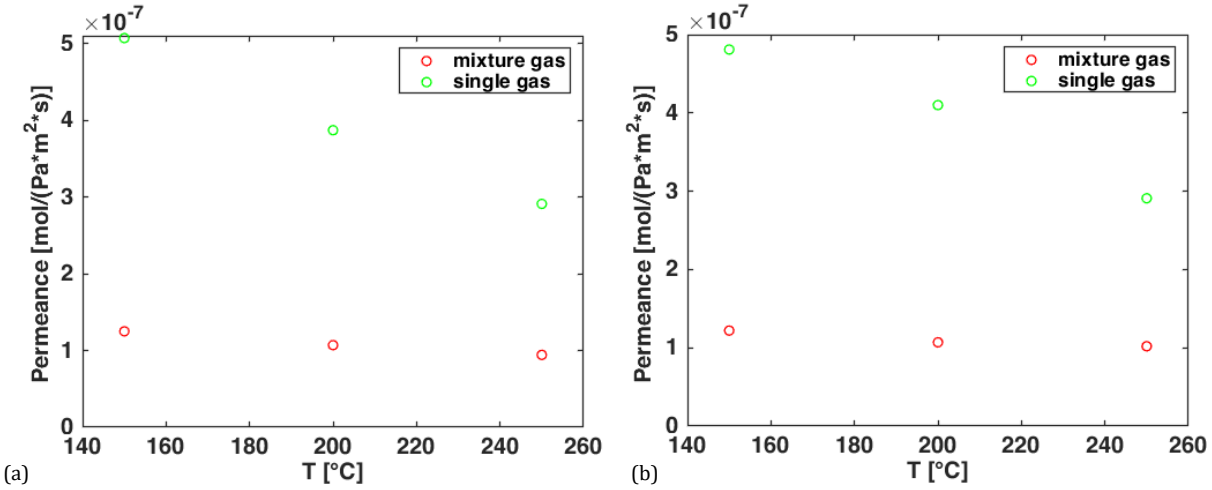

Figure 22: water permeance comparison between single vapor permeation test and vapor/gas mixture for CM700 (a) and CM600 (b)

The gas permeance, instead, increase with increasing operating temperature for H_2 and CO, which is a typical trend for Knudsen diffusion and molecular sieving mechanisms. CO_2 behaviour, however, is different, as it is depicted in Figure 23.

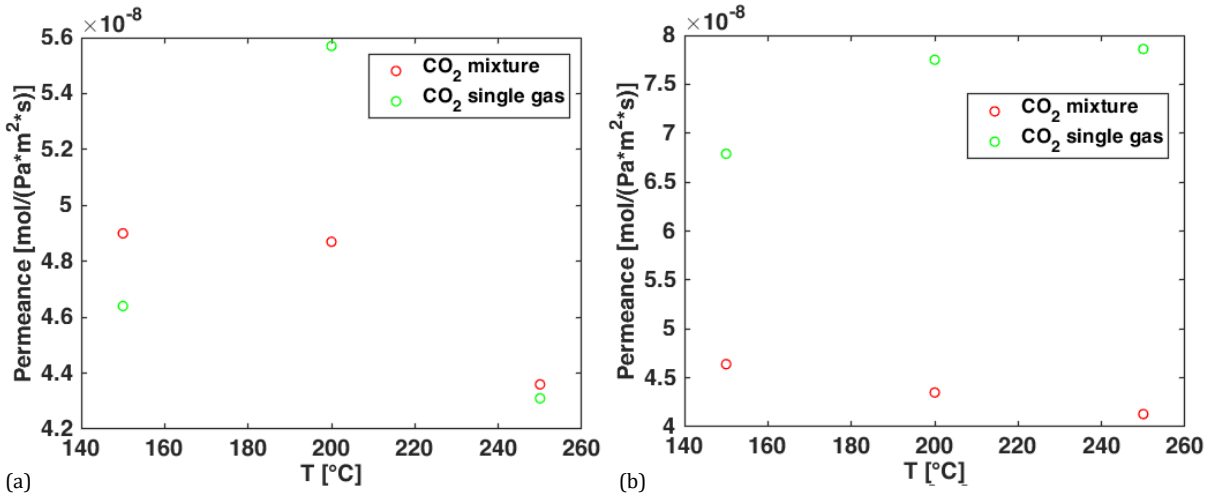

Figure 23: CO_2 permeance comparison between single gas permeation test and vapor/gas mixture for CM700 (a) and CM600 (b)

The permeance decreases very slightly with increasing operating temperature, which might be the reason of a rather constant H_2O/CO_2 selectivity. This is true for both membrane samples. Furthermore, it is possible to notice that for CM600, the permeance dependency

from temperature is different in single gas tests. This behaviour suggests a change in the main transport mechanism: it is likely that surface diffusion is the main transport in mixture. Moreover, the CO_2 permeance is also affected by its solubility in water. Thus, capillary condensation is also playing a role, as the higher amount of water in the pores, the higher the amount of CO_2 that solubilizes in it, resulting in a higher CO_2 flux through the membrane.

This is not the only different trend observed for CO_2. At lower operating temperature, when capillary condensation effect is more prominent, H_2O/CO_2 selectivity should be the lowest compared to H_2O/CO and H_2O/H_2 selectivity, as CO_2 is the most soluble molecule among the gases that have been studied. This is true for CM700 at 150°C operating temperature, but not always true when temperature increases. Furthermore, for CM600, the selectivity of CO_2 is comparable or higher than CO selectivity. Since CO_2 is smaller than CO, more soluble in water and more likely to be easily adsorbed on the membrane surface, a lower H_2O/CO_2 selectivity than CO would be expected.

To better understand the real selectivity trends for both membranes, especially H_2O/CO_2, ideal selectivities were calculated. However, as the CO bottle was empty at the time the ideal H_2O/CO selectivity needed to be measured for the membrane at 700°C carbonization temperature, these data are missing. Nonetheless, it is likely that the trend will be similar to the other sample, as all the other data are comparable between each other. The results are presented in Figure 24:

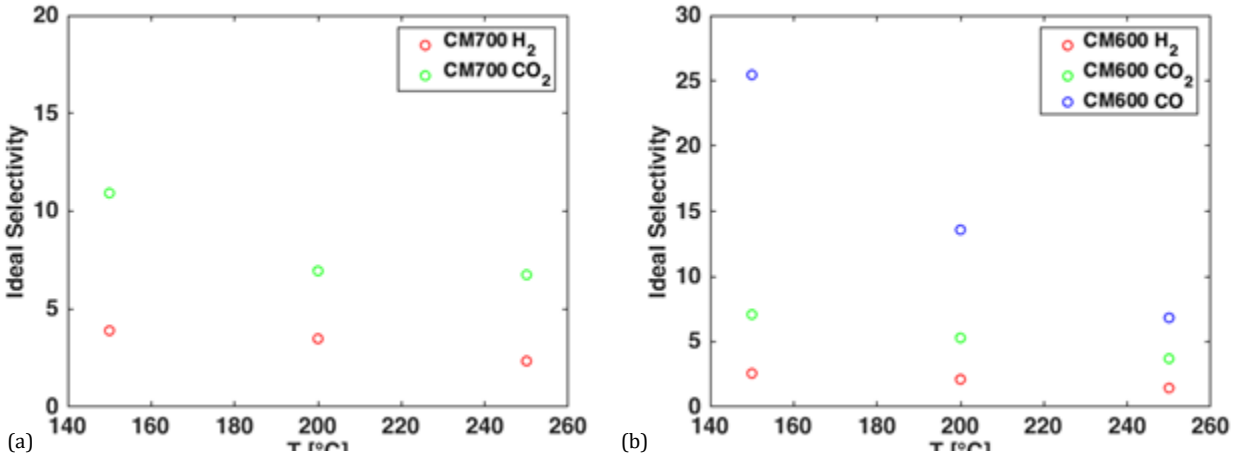

Figure 24: ideal selectivity for water/hydrogen, water/carbon dioxide and water/carbon monoxide (only for T_{carb}=600°C).

As it is possible to notice, the highest ideal selectivity is given for CO, which is the larger molecule in the system. As the ideal selectivity does not consider the interaction of the membrane with water, the selectivity towards hydrogen is the lowest.

However, these tests do not explain the H_2O/CO_2 selectivity trends when dealing with binary mixtures. One hypothesis that would explain this behaviour is that part of CO_2 of the system was loss during water condensation, due to the high solubility of the gas in water. Indeed, it

was observed that bubbles were still present in liquid water after condensation (Figure 25), therefore the gas concentration sent to the GC was likely to be less than the one that actually permeated through the membrane. To confirm this hypothesis, a water permeate sample and water retentate sample were analyzed via titration. The samples were collected after a H_2O/CO_2 permeation test on CM700 membrane at 150°C. Phenolphthalein was used as indicator and a 1M solution of sodium hydroxide was used as titrant. The amount of CO_2 found in the permeate sample was approximatively 37.5 mg/L, whereas in the retentate water sample, the CO_2 concentration was over 100 mg/L. This titration confirms the hypothesis that CO_2 does not completely desorbs from the permeated and retained water during the cooling procedure.

The selectivity was then corrected, with new values obtained being lower than the one previously calculated. This was a rather qualitative analysis and conducted for 150°C only on one membrane sample, in order to confirm that there is an actual CO_2 loss. Nonetheless, it can be concluded that the gas measurements of permeated gas flow and retentate composition are lower than the actual values. To solve this problem, a GC which is capable to feed liquid and gas should be used.

Figure 25: The picture on the left shows the result of the titration on the water permeate sample. The pink color shows that CO_2 is present in the sample. The picture on the right shows the gas bubble present in the permeate when the water is collected at room temperature.

Lastly, CO selectivity greatly decreases in binary mixture experiments. It was not possible to understand this behaviour, as it should be the molecule that can be retained the most, as it is less soluble than CO_2 and also the biggest molecule in the system.

6. Model prediction

The values of water permeance and selectivity determined experimentally, were implemented in the membrane reactor model, to assess the feasibility of the integration of a carbon membrane in a membrane reactor for the CO_2 hydrogenation to dimethyl ether. The main purpose is to show that the membrane reactor overcomes the thermodynamic limitation obtained with a conventional reactor.

The reactor geometry and operating conditions are the same for both the direct and indirect process and they are reported in Table 9:

Table 9: Summary of the most relevant reactor parameters used in the model.

Parameter	**Units**	**Value**
Operating temperature	°C	200
Operating pressure	bar	40
H_2/CO_2 feed ratio (direct)	mol/mol	3.5
H_2/CO_2 feed ratio (indirect)	mol/mol	3.0
Feed	mol/s	0.0015
Catalyst bed density (direct)	kg/m^3	1189.2
Catalyst bed density (indirect)	kg/m^3	447.46
Reactor length	m	1
Reactor diameter	m	0.0198

6.1. Direct route

First, real selectivity for all the gases are used whereas for water/methanol, ideal selectivity is the only possible choice. From the simulation, the predictions reported in Figure 26 (CM600) and Figure 27 (CM700) are obtained:

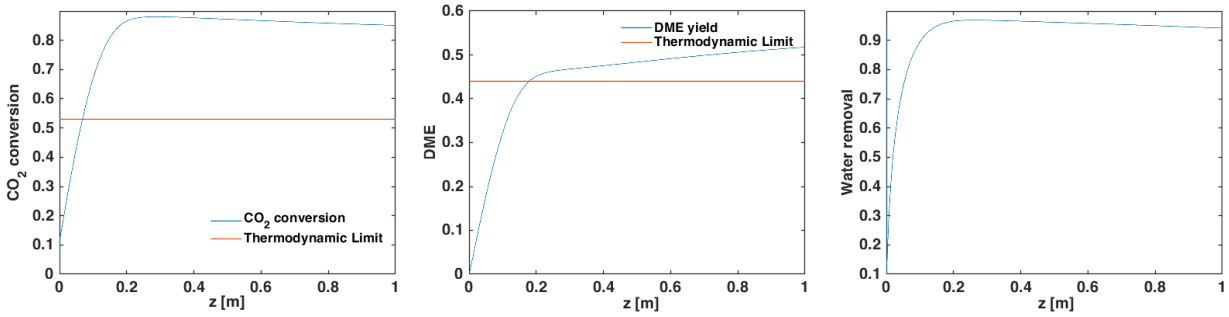

Figure 26: CO_2 conversion, DME yield and water removal fraction of a membrane reactor using the carbon membrane carbonized at 600°C (real selectivity for all gases).

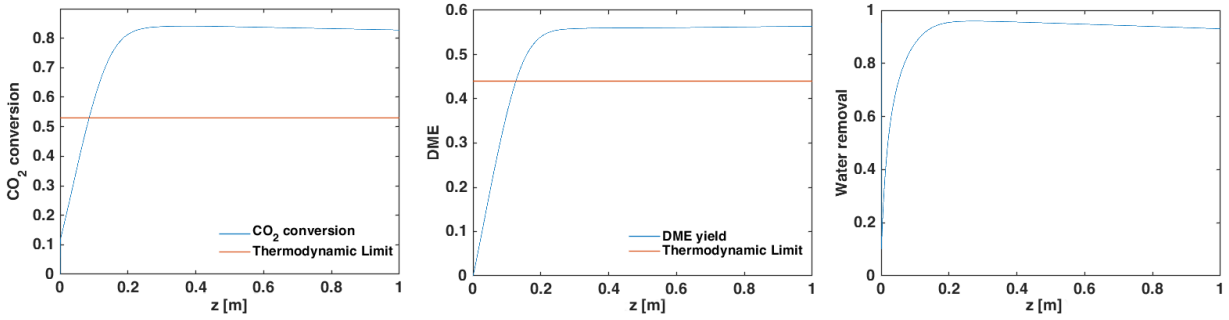

Figure 27: CO_2 conversion, DME yield and water removal fraction of a membrane reactor using the carbon membrane carbonized at 700°C (real selectivity for all gases).

As it is possible to notice when comparing Figure 26 and Figure 27, for both membrane reactors the fraction of water removed from the reaction zone approaches unity. This means that the water permeance obtained by these membranes is high enough to assure an almost dry reaction zone, with no excess water as byproduct. This removal leads, following Le Chatelier's principle, to an increase in carbon dioxide conversion, which overcomes the thermodynamic limitation of conventional reactors in both cases. In case of the membrane carbonized at lower temperature, the CO_2 conversion is slightly higher compared to the other sample. This difference depends on the real selectivity towards CO_2. Indeed, at T_{carb}=700°C, CO_2 selectivity is slightly lower, therefore a higher amount of reactant is lost in the permeation zone. This is well depicted in the figure below, where the CO_2 fraction in the permeate zone is plotted for both membrane samples.

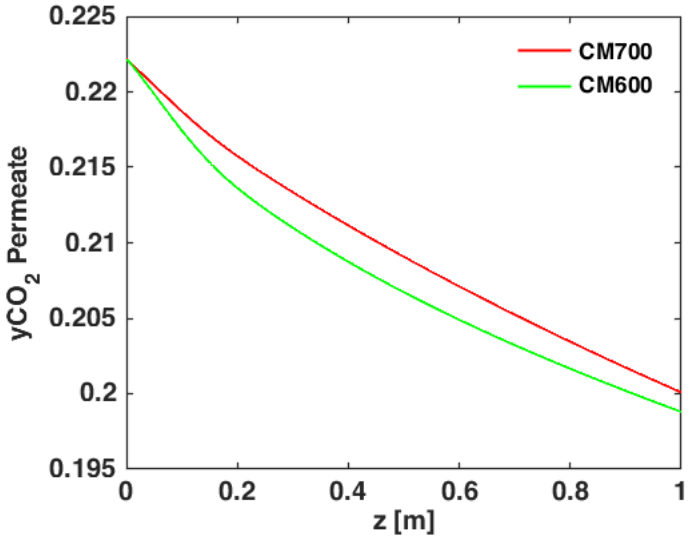

Figure 28: CO_2 fraction in the permeate zone for both membrane samples.

The DME yield is higher in the membrane reactor when implementing the membrane carbonized at higher temperature. The reason being that the ideal selectivity towards methanol is higher compared to the other sample, therefore more methanol can be further converted to DME. In both cases, the yield is above the thermodynamic limitation, although only slightly. The reason why the DME yield is still low depends on two different factors: first, the methanol selectivity is still low for this application, which means that methanol is lost in the permeation zone.

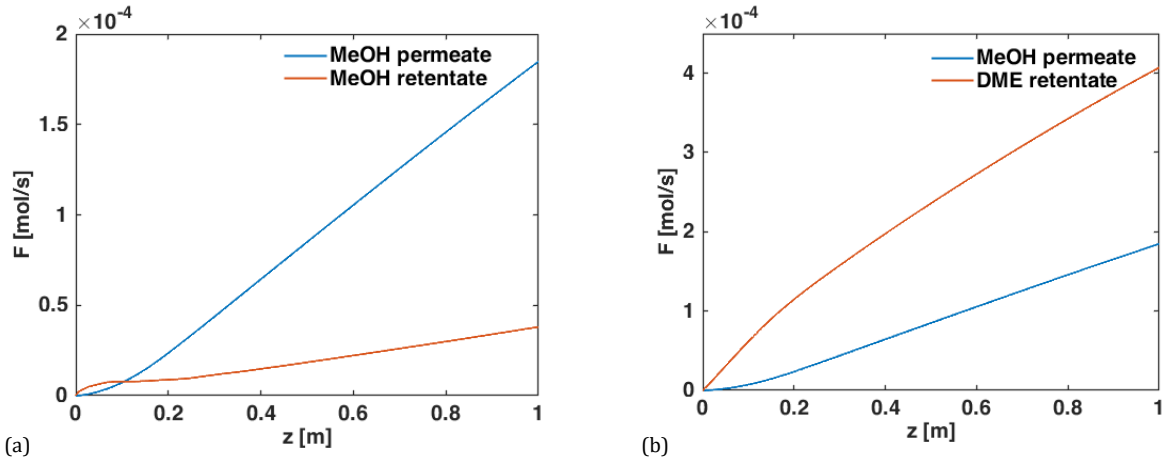

Figure 29: Methanol flowrate profiles in the permeation and in the reactor zone (a) and comparison between the methanol flowrate lost in the permeation zone and the produced DME flowrate in the reaction zone (b).

In Figure 29a the methanol flowrate in both permeation and reaction zone are reported. Here it is possible to easily notice that methanol significatively permeates along the reactor. In

Figure29b reports the methanol flowrate in the permeate zone compared to the product flowrate. This shows how much methanol could not be converted further to DME due to low selectivity towards methanol. However, as already highlighted, the selectivity obtained for both membranes are quite high compared to literature. Nonetheless, methanol loss accounts for low DME yield.

The second reason for low DME yield is the very low selectivity to CO. Since CO is a product of the RWGS reaction, which is an equilibrium reaction, its permeation through the membrane shifts the equilibrium towards the products. Thus, CO_2 tends to react more towards CO production, lowering down methanol yield and, therefore, DME yield.

The combination of methanol loss through the membrane and CO production reduce the overall DME yield. Both contributions are shown in Figure 30, where it is possible to see how higher H_2O/CO selectivity in CM700 results in a decrease in CO yield, compared to CM600. Indeed, for the membrane CM600, CO and MeOH yield increase, as their permeation enhances their production in the reaction zone. For this sample, both H_2O/MeOH and H_2O/CO selectivity are lower compared to CM700.

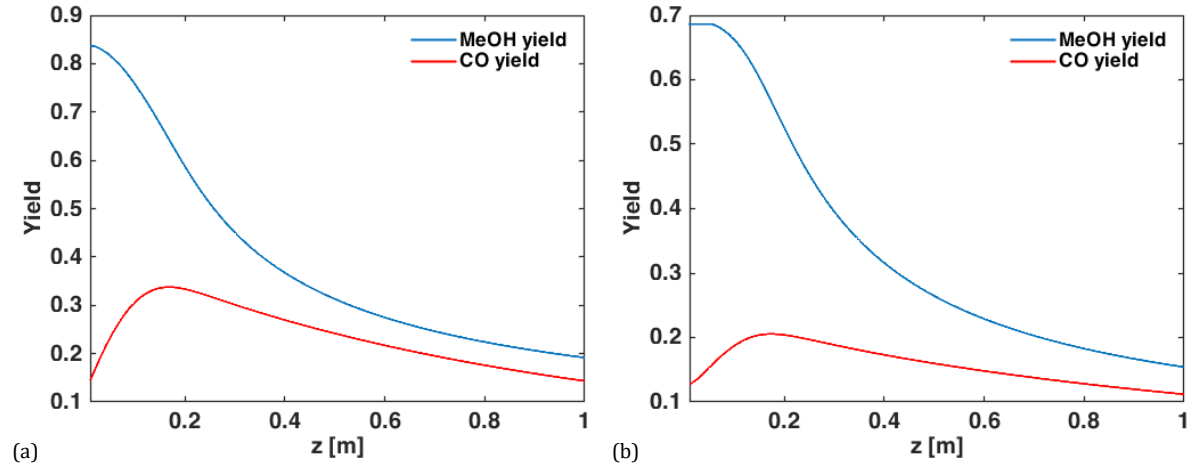

Figure 30: Methanol yield and CO yield for the membrane sample carbonized at T=600°C (a) and T=700°C (b)

To further confirm the role of H_2O/CO selectivity in the DME yield decrease, the ideal selectivity towards CO was used for the next simulation, while all the others were kept the same. The results obtained from the simulation are the one depicted in Figure 31 and Figure 32:

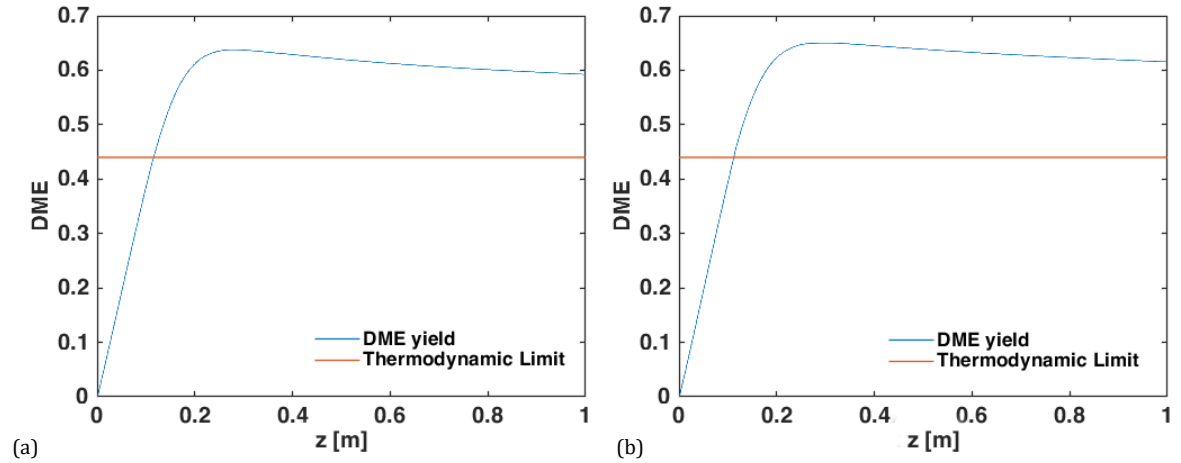

Figure 31: DME yield of a membrane reactor using the carbon membrane carbonized at 600°C (a) and carbonized at 700°C (b).

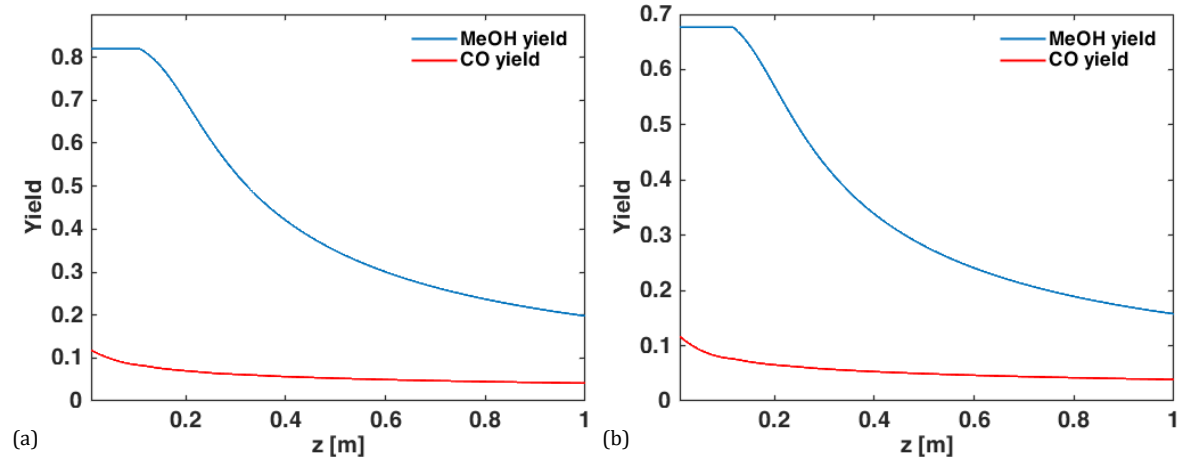

Figure 32: MeOH and CO yield of a membrane reactor using the carbon membrane carbonized at 600°C (a) and 700°C (b).

Compared to the simulation in which CO real selectivity is used, the main noticeable difference is the increase in DME yield. Indeed, the overall performance is improved. Moreover, CO yield decreased compared to the previous case. Thus, these results confirm as CO selectivity plays an important role in DME yield, as all selectivity used for this run were the same used for the previous simulations.

From the comparison between the two membranes, the membrane carbonized at 700°C seems to have the best performance in terms of DME yield. This is mainly due to a higher water/methanol selectivity, which leads to lower methanol yield, and the higher water/CO selectivity in both the real case and, likely, in the ideal case. Therefore, this membrane should be preferred. However, the methanol yield is still high, thus the water/methanol selectivity should be higher in order to avoid methanol loss in the permeate.

6.2. Indirect route

As for the previous section, the real selectivity were firstly used in the reactor model to predict the reactor performance. In order to compare both models, the same geometry, number of membranes and inlet flowrate were used. In this way, the residence time of both reactors is kept the same.

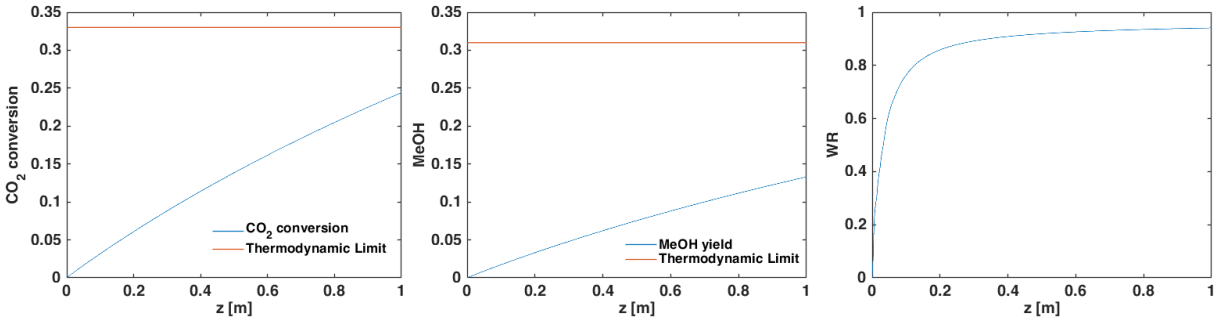

Figure 33: CO_2 conversion, MeOH yield and water removal fraction of a membrane reactor using the carbon membrane carbonized at 600°C (real selectivity for all gases).

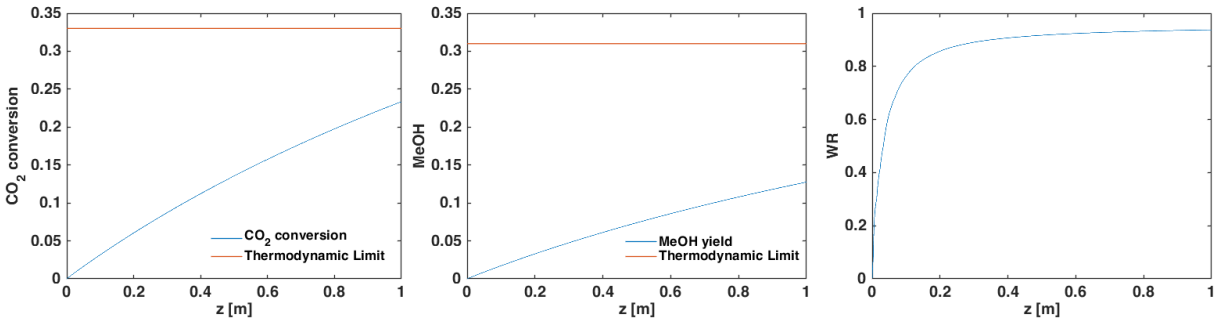

Figure 34: CO_2 conversion, MeOH yield and water removal fraction of a membrane reactor using the carbon membrane carbonized at 700°C (real selectivity for all gases).

From Figure 33 and Figure 34 the first thing to notice is that the residence time is not long enough to reach the steady state. Therefore, a lower flowrate or a longer reactor should be used for comparison. The higher residence time depends on a slower reaction rate compared to the direct process, where MeOH production is boosted by its conversion into DME. Moreover, it is possible to see that the two membranes behave almost the same, which makes sense as the membranes have comparable water permeance. In the methanol yield calculation, also the methanol present in the permeation zone is considered, as it can be separated from the water permeate in downstream treatment and fed into the second reactor to produce DME.

Another difference is the slight increase in CO_2 conversion in the membrane sample with lower carbonization temperature. This is mainly due to the lower CO selectivity. As CO is consumed to produce methanol but it is also produced from reverse water gas shift, lower selectivity boosts the CO production in the RWGS reaction and then it can be converted in methanol.

After this run, the flowrate was lowered down to reach steady state. It was successfully reached for the membrane carbonized at 700°C, which is the preferred membrane sample.

The results of the simulation are shown in Figure 35:

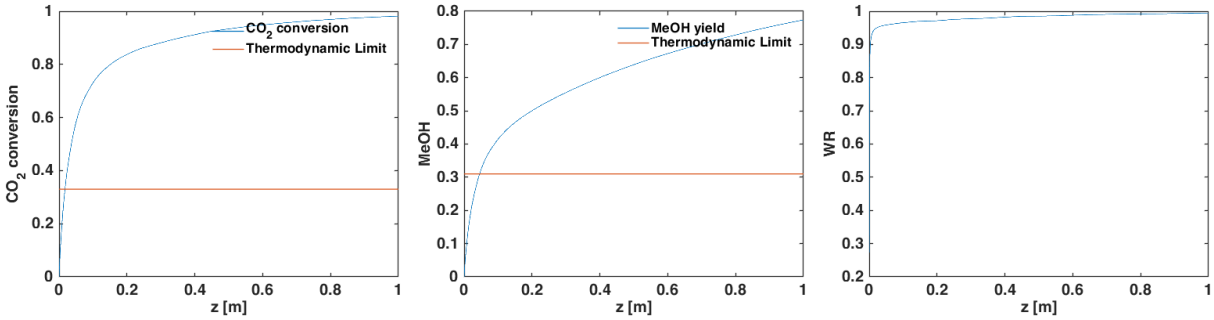

Figure 35: CO_2 conversion, MeOH yield and water removal fraction of a membrane reactor using the carbon membrane carbonized at 700°C (steady state reached).

The flowrate had to be lowered from 0.0015 m/s to 0.000015 m/s to reach steady state. Considering the steady state for CM700, the methanol yield is close to 80%. However, not all the methanol produced will be converted into DME. As previously assumed (Chapter 3, Section 6.1), only 85% of methanol will be converted into DME. Thus, the DME yield would be around 68% at maximum, which is slightly higher compared to the yield obtained with the direct synthesis model. Nonetheless, this slight increase comes with higher capital costs: the reactor needed to reach the same productivity has to be larger, as the residence time is higher in the indirect route for the first step. Moreover, a second reactor is required, with a methanol recovery stage in between. This increase in capital cost may not justify the 10% yield increase compared to the direct synthesis, which has also a larger productivity, as the residence time is shorter.

Chapter 5
Conclusions

The aim of this project was to assess the feasibility of the integration of carbon membranes in a packed bed reactor for DME synthesis from CO_2 and H_2. Since carbon membrane properties are very sensitive to their synthesis conditions, their performances can vary depending on different parameters. One of the main parameters that can affect membrane performance is the carbonization temperature. Thus, in this project, the effect of carbonization temperature on two membrane samples was assessed.

What has been found is that increasing the carbonization temperature from 600°C to 700°C leads to a shrink in the pore size and a change in the amount and types of functional groups on the carbon layer. The smaller pore size leaded to a decrease in the permeation fluxes and increase in the selectivity as a general trend. The presence of different functional group with increasing carbonization temperature leaded to a more hydrophilic membrane, which lead to a comparable water permeation flux between CM600 and CM700 membrane samples.

In case of pure water vapor permeation tests, however, the overall permeance was comparable between the two membranes. The reason being that the main phenomenon which drives water permeation is capillary condensation. Capillary condensation is driven by both pressure changes, depending on the pore size, and membrane hydrophilicity. The similar permeance in the two samples suggested that this phenomenon is happening at comparable rate. The reason being that the two aforementioned effects are likely compensating for each other, leading to similar results.

The difference in the pore size and in the membrane affinity to water affects the permeation and selectivity of methanol and binary mixtures the most. Especially when dealing with methanol, a higher carbonization temperature leaded to a higher methanol selectivity. This higher selectivity is desired if the membrane reactor will be used for direct DME synthesis processes.

The experimental results were then implemented in an isothermal 1D-reactor model to assess the performance of a packed bed membrane reactor. The results obtained were then compared to the thermodynamic limit of a conventional packed bed reactor, operating at the same conditions. The results showed that the implementation of a carbon membrane for the direct process might be more beneficial than for the indirect process, as it has shorter residence time, which leads to a capital cost reduction. Moreover, the obtainable DME yield is only maximum 10% lower when it is produced via direct route and depends mainly on methanol loss, which can be overcame by increasing the selectivity towards methanol.

Both the membranes were capable to overcome the thermodynamic limitation for the DME yield when real selectivity for all gases were used.

Thus, carbon membranes are a promising candidate for industrial application, as far as the H_2O/CO selectivity is high enough. Specifically, the membrane samples used in this project have shown very low H_2O/CO and H_2O/CO_2 selectivity, which is not desirable for industrial application. Nonetheless, the $H_2O/MeOH$ selectivity was high enough to allow their use in direct process application. Moreover, the permeation of these components could be also avoided by feeding them through the sweep gas, in order to control their driving force.

Outlook

In order to improve the findings of this project, a more detailed analysis on the pore size distribution of the membrane should be conducted. It is likely that using CO_2 adsorption rather than nitrogen adsorption method will highlight smaller pores that were not visible with the used equipment. Moreover, the CO ideal selectivity for the membrane sample carbonized at 700°C should be measured, to confirm that it is indeed higher than the one of the other sample.

The studies on binary mixtures should be repeated. Indeed, CO results are likely to suffer from experimental error, most likely due to wrong GC calibration. Moreover, effort should be made to test binary mixtures in adequate setup, due to CO_2 loss in water during condensation. This problem can be solved by having an analyzer capable to handle both liquid and gas simultaneously.

As regards to the model, the first improvement should be to verify that choosing a different composition of sweep gas, including MeOH and CO, may improve the reactor performance even at low selectivity. Moreover, energy balances and pressure drops should be added to the indirect model as it has been done for the direct model from the model developer.

Lastly, more membranes should be tested at a wider carbonization temperature range, in a wider operating temperature range, to fully understand the effects that this parameter has on the membrane performances. Two samples are not enough to draw precise conclusions.

Acknowledgements

I always wonder what to write in this section throughout my two years in TU/e. Today, I believe that my gratitude is the only thing that matters. This report is the result of ten months spent within the SPE labs, and I would like to thank the whole SPE-SIR and SPE-CRE research groups for letting me feel like I was part of the team and not only a student. I cherish wonderful moments with you, both educational and playful ones.

I would like to express my sincere gratitude to my supervisors, Prof. Dr. Eng. Fausto Gallucci and Dr. Fernanda Neira d'Angelo, for helping me throughout the whole duration of my project, for their guidance and their support. A special thank goes to Serena Poto, my daily supervisor, for her patience and her constant support, inside and outside university.

Living abroad was not an easy task, especially in 2020, but I had my friends here. They were always there to light up the way, and always had my back. For this reason, I want to thank Abhishek, Michele, Simone and the "new addition" Appi and Serena, which helped me throughout this journey.

Last, but certainly not least, I want to dedicate this thesis to my dad, my mum, Myriam and Fabio, for whom I feel deeply grateful. I am grateful for the sacrifices you made to support my dreams, for the faith you always had in me, for the love we share. No matter how far we are, no matter how far we will go, we will always be together.

Thank you.

Bibliography

[1] S. Shafiee and E. Topal, “An econometrics view of worldwide fossil fuel consuption and role of US,” *Energy Policy*, vol. 36, pp. 775–786, 2008.

[2] T. R. Anderson, E. Hawkins, and P. D. Jones, “CO2, the greenhouse effect and global warming: from the pioneering work of Arrhenius and Callendar to today’s Earth System Models,” *Endeavour*, vol. 40, no. 3, pp. 178–187, 2016.

[3] S. Ó. Snæbjörnsdóttir, B. Sigfússon, C. Marieni, D. Goldberg, S. R. Gislason, and E. H. Oelkers, “Carbon dioxide storage through mineral carbonation,” *Nat. Rev. Earth Environ.*, vol. 1, no. 2, pp. 90–102, 2020.

[4] Y. Tan, W. Nookuea, H. Li, E. Thorin, and J. Yan, “Property impacts on Carbon Capture and Storage (CCS) processes: A review,” *Energy Convers. Manag.*, vol. 118, pp. 204–222, 2016.

[5] G. Centi and S. Perathoner, “Opportunities and prospects in the chemical recycling of carbon dioxide to fuels,” *Catal. Today*, vol. 148, no. 3–4, pp. 191–205, 2009.

[6] T. A. Semelsberger, R. L. Borup, and H. L. Greene, “Dimethyl ether (DME) as an alternative fuel,” *J. Power Sources*, vol. 156, no. 2, pp. 497–511, 2006.

[7] M. De Falco, M. Capocelli, and A. Basile, “Selective membrane application for the industrial one-step DME production process fed by CO2 rich streams: Modeling and simulation,” *Int. J. Hydrogen Energy*, vol. 42, no. 10, pp. 6771–6786, 2017.

[8] C. Arcoumanis, C. Bae, R. Crookes, and E. Kinoshita, “The potential of di-methyl ether (DME) as an alternative fuel for compression-ignition engines: A review,” *Fuel*, vol. 87, no. 7, pp. 1014–1030, 2008.

[9] Q. Zhang, X. Li, K. Fujimoto, and K. Asami, “Hydrogen production by partial oxidation and reforming of DME,” *Appl. Catal. A Gen.*, vol. 288, no. 1–2, pp. 169–174, 2005.

[10] M. Xu, J. H. Lunsford, D. W. Goodman, and A. Bhattacharyya, “Synthesis of dimethyl ether (DME) from methanol over solid-acid catalysts,” *Appl. Catal. A Gen.*, vol. 149, no. 2, pp. 289–301, 1997.

[11] J. Wu, M. Saito, M. Takeuchi, and T. Watanabe, “The stability of Cu/ZnO-based catalysts in methanol synthesis from a CO2-rich feed and from a CO-rich feed,” *Appl. Catal. A Gen.*, vol. 218, no. 1–2, pp. 235–240, 2001.

[12] M. De Falco, M. Capocelli, and A. Giannattasio, “Membrane Reactor for one-step DME synthesis process: Industrial plant simulation and optimization,” *J. CO2 Util.*, vol. 22, no. September, pp. 33–43, 2017.

[13] F. Gallucci and A. Basile, “A theoretical analysis of methanol synthesis from CO2 and H2 in a ceramic membrane reactor,” *Int. J. Hydrogen Energy*, vol. 32, no. 18, pp. 5050–5058, 2007.

[14] A. F. Ismail and L. I. B. David, “A review on the latest development of carbon membranes for gas separation,” *J. Memb. Sci.*, vol. 193, no. 1, pp. 1–18, 2001.

[15] C. W. Jones and W. J. Koros, “Carbon Composite Membranes: A Solution to Adverse Humidity Effects,” *Ind. Eng. Chem. Res.*, vol. 34, no. 1, pp. 164–167, 1995.

[16] M. G. Sedigh, W. J. Onstot, L. Xu, W. L. Peng, T. T. Tsotsis, and M. Sahimi, “Experiments and simulation of transport and separation of gas mixtures in carbon molecular sieve membranes,” *J. Phys. Chem. A*, vol. 102, no. 44, pp. 8580–8589, 1998.

[17] A. Tavolaro and E. Drioli, “Zeolite membranes,” *Adv. Mater.*, vol. 11, no. 12, pp. 975–996, 1999.

[18] J. B. S. Hamm, A. Ambrosi, J. G. Griebeler, N. R. Marcilio, I. C. Tessaro, and L. D. Pollo, “Recent advances in the development of supported carbon membranes for gas separation,” *Int. J. Hydrogen Energy*, vol. 42, no. 39, pp. 24830–24845, 2017.

[19] F. Gallucci, L. Paturzo, and A. Basile, “An experimental study of CO2 hydrogenation into methanol involving a zeolite membrane reactor,” *Chem. Eng. Process. Process Intensif.*, vol. 43, no. 8, pp. 1029–1036, 2004.

[20] N. Diban, A. M. Urtiaga, I. Ortiz, J. Ereña, J. Bilbao, and A. T. Aguayo, “Influence of the membrane properties on the catalytic production of dimethyl ether with in situ water removal for the successful capture of co2,” *Chem. Eng. J.*, vol. 234, pp. 140–148, 2013.

[21] R. Xu *et al.*, “Ultraselective carbon molecular sieve membrane for hydrogen purification,” *J. Energy Chem.*, vol. 50, pp. 16–24, 2020.

[22] A. B. Fuertes, “Adsorption-selective carbon membrane for gas separation,” *J. Memb. Sci.*, vol. 177, no. 1–2, pp. 9–16, 2000.

[23] C. Liang, G. Sha, and S. Guo, “Carbon membrane for gas separation derived from coal tar pitch,” *Carbon N. Y.*, vol. 37, no. 9, pp. 1391–1397, 1999.

[24] W. N. W. Salleh and A. F. Ismail, “Carbon membranes for gas separation processes: Recent progress and future perspective,” *J. Membr. Sci. Res.*, vol. 1, no. 1, pp. 2–15, 2015.

[25] W. Wei, G. Qin, H. Hu, L. You, and G. Chen, “Preparation of supported carbon molecular sieve membrane from novolac phenol-formaldehyde resin,” *J. Memb. Sci.*, vol. 303, no. 1–2, pp. 80–85, 2007.

[26] F. Gallucci, E. Fernandez, P. Corengia, and M. van Sint Annaland, “Recent advances on membranes and membrane reactors for hydrogen production,” *Chem. Eng. Sci.*, vol. 92, pp. 40–66, 2013.

[27] T. A. Centeno and A. B. Fuertes, “Carbon molecular sieve membranes derived from a phenolic resin supported on porous ceramic tubes,” *Sep. Purif. Technol.*, vol. 25, no. 1–3, pp. 379–384, 2001.

[28] T. A. Centeno and A. B. Fuertes, “Supported carbon molecular sieve membranes based on a phenolic resin,” *J. Memb. Sci.*, vol. 160, no. 2, pp. 201–211, 1999.

[29] A. S. Damie, S. K. Gangwal, J. J. Spivey, J. Longanbach, and V. K. Venkataraman, “Carbon membranes for gas separation,” *Key Eng. Mater.*, vol. 61–62, no. 3, pp. 273–278, 1991.

[30] P. Uchytil, R. Petrickovic, S. Thomas, and A. Seidel-Morgenstern, “Influence of capillary condensation effects on mass transport through porous membranes,” *Sep. Purif. Technol.*,

vol. 33, no. 3, pp. 273–281, 2003.

[31] R. J. R. Uhlhorn, K. Keizer, and A. J. Burggraaf, “Gas transport and separation with ceramic membranes. Part I. Multilayer diffusion and capillary condensation,” *J. Memb. Sci.*, vol. 66, no. 2–3, pp. 259–269, 1992.

[32] K. H. Lee and S. T. Hwang, “The transport of condensible vapors through a microporous vycor glass membrane,” *J. Colloid Interface Sci.*, vol. 110, no. 2, pp. 544–555, 1986.

[33] S. Sommer and T. Melin, “Influence of operation parameters on the separation of mixtures by pervaporation and vapor permeation with inorganic membranes. Part 1: Dehydration of solvents,” *Chem. Eng. Sci.*, vol. 60, no. 16, pp. 4509–4523, 2005.

[34] Z. Azizi, M. Rezaeimanesh, T. Tohidian, and M. R. Rahimpour, “Dimethyl ether: A review of technologies and production challenges,” *Chem. Eng. Process. Process Intensif.*, vol. 82, pp. 150–172, 2014.

[35] R. Ladera, E. Finocchio, S. Rojas, J. L. G. Fierro, and M. Ojeda, “Supported niobium catalysts for methanol dehydration to dimethyl ether: FTIR studies of acid properties,” *Catal. Today*, vol. 192, no. 1, pp. 136–143, 2012.

[36] L. Zhang, J. Wang, P. Wu, Z. Hou, J. Fei, and X. Zheng, “Synthesis of dimethyl ether via methanol dehydration over combined Al2O3-HZSM-5 solid acids,” *Cuihua Xuebao/Chinese J. Catal.*, vol. 31, no. 8, pp. 987–992, 2010.

[37] F. Raoof, M. Taghizadeh, A. Eliassi, and F. Yaripour, “Effects of temperature and feed composition on catalytic dehydration of methanol to dimethyl ether over γ-alumina,” *Fuel*, vol. 87, no. 13–14, pp. 2967–2971, 2008.

[38] E. F. Sousa-Aguiar, L. G. Appel, and C. Mota, “Natural gas chemical transformations: The path to refining in the future,” *Catal. Today*, vol. 101, no. 1, pp. 3–7, 2005.

[39] Y. Wang, W. L. Wang, Y. X. Chen, J. J. Zheng, and R. F. Li, “Synthesis of dimethyl ether from syngas using a hierarchically porous composite zeolite as the methanol dehydration catalyst,” *Ranliao Huaxue Xuebao/Journal Fuel Chem. Technol.*, vol. 41, no. 7, pp. 875–882, 2013.

[40] W. Z. Lu, L. H. Teng, and W. De Xiao, “Simulation and experiment study of dimethyl ether synthesis from syngas in a fluidized-bed reactor,” *Chem. Eng. Sci.*, vol. 59, no. 22–23, pp. 5455–5464, 2004.

[41] I. Iliuta, F. Larachi, and P. Fongarland, “Dimethyl ether synthesis with in situ H2o removal in fixed-bed membrane reactor: Model and simulations,” *Ind. Eng. Chem. Res.*, vol. 49, no. 15, pp. 6870–6877, 2010.

[42] K. M. Vanden Bussche and G. F. Froment, “A steady-state kinetic model for methanol synthesis and the water gas shift reaction on a commercial Cu/ZnO/Al2O3 catalyst,” *J. Catal.*, vol. 161, no. 1, pp. 1–10, 1996.

[43] M. P. Rohde, D. Unruh, and G. Schaub, “Membrane application in Fischer-Tropsch synthesis to enhance CO2 hydrogenation,” *Ind. Eng. Chem. Res.*, vol. 44, no. 25, pp. 9653–9658, 2005.

[44] J. F. Portha *et al.*, “Kinetics of Methanol Synthesis from Carbon Dioxide Hydrogenation

over Copper-Zinc Oxide Catalysts," *Ind. Eng. Chem. Res.*, vol. 56, no. 45, pp. 13133–13145, 2017.

[45] G. H. Graaf, H. Scholtens, E. J. Stamhuis, and A. A. C. M. Beenackers, "Intra-particle diffusion limitations in low-pressure methanol synthesis," *Chem. Eng. Sci.*, vol. 45, no. 4, pp. 773–783, 1990.

[46] X. Feng and R. Y. M. Huang, "Estimation of activation energy for permeation in pervaporation processes," *J. Memb. Sci.*, vol. 118, no. 1, pp. 127–131, 1996.

[47] H. B. Park, J. Kamcev, L. M. Robeson, M. Elimelech, and B. D. Freeman, "Maximizing the right stuff: The trade-off between membrane permeability and selectivity," *Science (80-.).*, vol. 356, no. 6343, pp. 1138–1148, 2017.

[48] L. M. Robeson, "Correlation of separation factor versus permeability for polymeric membranes," *J. Memb. Sci.*, vol. 62, no. 2, pp. 165–185, 1991.

[49] D. Y. Zhang, H. T.; Cao, F. H.; Liu, D. H.; Fang, "Thermodynamic analysis for synthesis of dimethyl ether and methanol from synthesis gas," *J. ECUST*, vol. 27, pp. 198–201, 2001.

[50] https://www.sigmaaldrich.com/technical-documents/articles/biology/ir-spectrum-table.html

Appendix A: permeation tests

1. Water permeation

CM700	150°C	200°C	250°C
Test 1	$4.70 \cdot 10^{-7}$	$3.99 \cdot 10^{-7}$	$2.85 \cdot 10^{-7}$
Test 2	$5.44 \cdot 10^{-7}$	$3.76 \cdot 10^{-7}$	$2.96 \cdot 10^{-7}$
Mean Permeance	$5.07 \cdot 10^{-7}$	$3.87 \cdot 10^{-7}$	$2.91 \cdot 10^{-7}$

CM600	150°C	200°C	250°C
Test 1	$4.81 \cdot 10^{-7}$	$3.87 \cdot 10^{-7}$	$2.85 \cdot 10^{-7}$
Test 2	$4.81 \cdot 10^{-7}$	$4.33 \cdot 10^{-7}$	$2.96 \cdot 10^{-7}$
Mean Permeance	$4.81 \cdot 10^{-7}$	$4.10 \cdot 10^{-7}$	$2.91 \cdot 10^{-7}$

2. Methanol permeation

CM700	150°C	200°C	270°C
Test 1	$9.17 \cdot 10^{-8}$	$6.76 \cdot 10^{-8}$	$6.27 \cdot 10^{-8}$
Test 2	$8.69 \cdot 10^{-8}$	$7.24 \cdot 10^{-8}$	$5.79 \cdot 10^{-8}$
Mean Permeance	$8.93 \cdot 10^{-8}$	$7.00 \cdot 10^{-8}$	$6.03 \cdot 10^{-8}$

To calculate the mean permeance at 250°C, the trendline equation is used:

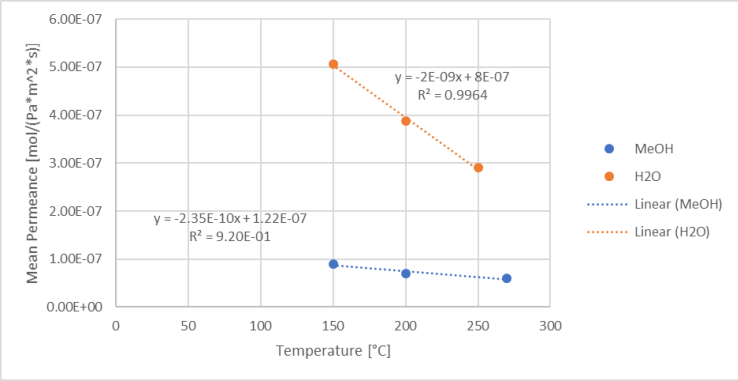

$y = -2.35 \cdot 10^{-10} \cdot 250 + 1.22 \cdot 10^{-7}$

$y = 6.33 \cdot 10^{-8}$

CM600	150°C	200°C	250°C
Test 1	$1.06 \cdot 10^{-7}$	$9.65 \cdot 10^{-8}$	$8.20 \cdot 10^{-8}$
Test 2	$1.01 \cdot 10^{-7}$	$9.17 \cdot 10^{-8}$	$8.20 \cdot 10^{-8}$
Mean Permeance	$1.04 \cdot 10^{-7}$	$9.41 \cdot 10^{-8}$	$8.20 \cdot 10^{-8}$

3. Ideal Selectivity

H_2O/MeOH	*S* [T=150°C]	*S* [T=200°C]	*S* [T=250°C]
CM700	5.678	5.529	4.598
CM600	4.625	4.357	3.549

CO_2	P [T=150°C]	P [T=200°C]	P [T=250°C]
CM700	$4.64 \cdot 10^{-8}$	$5.57 \cdot 10^{-8}$	$4.31 \cdot 10^{-8}$
CM600	$6.79 \cdot 10^{-8}$	$7.75 \cdot 10^{-8}$	$7.8 \cdot 10^{-8}$

H_2O/CO_2	*S* [T=150°C]	*S* [T=200°C]	*S* [T=250°C]
CM700	10.93	6.95	6.75
CM600	7.09	5.29	3.70

H_2	P [T=150°C]	P [T=200°C]	P [T=250°C]
CM700	$1.30 \cdot 10^{-7}$	$1.11 \cdot 10^{-7}$	$1.24 \cdot 10^{-7}$
CM600	$1.87 \cdot 10^{-7}$	$1.94 \cdot 10^{-7}$	$2.01 \cdot 10^{-7}$

H_2O/H_2	S [T=150°C]	S [T=200°C]	S [T=250°C]
CM700	3.90	3.49	2.35
CM600	2.57	2.11	1.45

CO	P [T=150°C]	P [T=200°C]	P [T=250°C]
CM700	-	-	-
CM600	$1.89 \cdot 10^{-8}$	$3.02 \cdot 10^{-8}$	$4.26 \cdot 10^{-8}$

H_2O/CO	S [T=150°C]	S [T=200°C]	S [T=250°C]
CM700	-	-	-
CM600	25.45	13.58	6.83

4. Real Selectivity

Due to setup limitation, it was not possible to evaluate the permeate gas composition directly. The known data were:

- Inlet feed flowrate and composition
- Retentate gas composition
- Permeate gas flowrate.

To evaluate the real selectivity of the mixture, the permeate gas composition is needed. This was analytically evaluated. First, an overall balance on the gas flowrates was written, as:

$$\Phi_i^F = \Phi_i^P + \Phi_i^R = y_i^P * \Phi_{N_2+i}^P + y_i^R * \Phi_{N_{2+i}}^R \qquad \textit{Eq. 48}$$

The unknown in this balance, however, are two: the permeate gas fraction and the cumulative retentate flowrate. Therefore, a second balance on the overall gas and nitrogen flowrates was computed:

$$\Phi_i^F + \Phi_{N_2}^F = \Phi_{N_2+i}^P + \Phi_{N_2+i}^R \qquad \textit{Eq. 49}$$

From the second balance, it is possible to calculate the overall gas retentate flowrate, thus, the permeate gas fraction is expressed as:

$$y_{GAS}^{P} = \frac{\Phi_i^F - y_i^R * \Phi_{N_2+i}^R}{\Phi_{N_2+i}^P} \qquad \textit{Eq. 50}$$

CM600 CO_2	150°C	200°C	250°C
Test 1 CO_2	$4.646 \cdot 10^{-8}$	$4.306 \cdot 10^{-8}$	$4.104 \cdot 10^{-8}$
Test 1 H_2O	$1.257 \cdot 10^{-7}$	$1.124 \cdot 10^{-7}$	$1.021 \cdot 10^{-7}$
Test 2 CO_2	$4.631 \cdot 10^{-8}$	$4.397 \cdot 10^{-8}$	$4.157 \cdot 10^{-8}$
Test 2 H_2O	$1.193 \cdot 10^{-7}$	$1.04 \cdot 10^{-7}$	$1.021 \cdot 10^{-7}$
Selectivity	2.64	2.49	2.47

CM600 H_2	150°C	200°C	250°C
Test 1 H_2	$4.155 \cdot 10^{-8}$	$5.003 \cdot 10^{-8}$	$5.724 \cdot 10^{-8}$
Test 1 H_2O	$1.595 \cdot 10^{-7}$	$1.286 \cdot 10^{-7}$	$9.636 \cdot 10^{-8}$
Test 2 H_2	$4.054 \cdot 10^{-8}$	$5.333 \cdot 10^{-8}$	$4.863 \cdot 10^{-8}$
Test 2 H_2O	$1.492 \cdot 10^{-7}$	$1.281 \cdot 10^{-7}$	$1.056 \cdot 10^{-7}$
Selectivity	3.76	2.49	1.93

CM600 CO	150°C	200°C	250°C
Test 1 CO	$6.536 \cdot 10^{-8}$	$9.752 \cdot 10^{-8}$	$9.172 \cdot 10^{-8}$
Test 1 H_2O	$1.140 \cdot 10^{-7}$	$8.905 \cdot 10^{-8}$	$8.342 \cdot 10^{-8}$
Test 2 CO	$6.475 \cdot 10^{-8}$	$9.604 \cdot 10^{-8}$	$8.953 \cdot 10^{-8}$
Test 2 H_2O	$1.233 \cdot 10^{-7}$	$8.811 \cdot 10^{-8}$	$8.934 \cdot 10^{-8}$
Selectivity	1.82	0.92	0.95

CM700 CO_2	150°C	200°C	250°C
Test 1 CO_2	$4.997 \cdot 10^{-8}$	$4.843 \cdot 10^{-8}$	$4.345 \cdot 10^{-8}$
Test 1 H_2O	$1.190 \cdot 10^{-7}$	$1.031 \cdot 10^{-7}$	$8.771 \cdot 10^{-8}$
Test 2 CO_2	$4.814 \cdot 10^{-8}$	$4.899 \cdot 10^{-8}$	$4.378 \cdot 10^{-8}$
Test 2 H_2O	$1.172 \cdot 10^{-7}$	$1.031 \cdot 10^{-7}$	$8.499 \cdot 10^{-8}$
Selectivity	2.41	2.12	1.98

CM700 H_2	150°C	200°C	250°C
Test 1 H_2	$6.119 \cdot 10^{-8}$	$5.242 \cdot 10^{-8}$	$6.054 \cdot 10^{-8}$
Test 1 H_2O	$9.462 \cdot 10^{-8}$	$1.092 \cdot 10^{-7}$	$9.408 \cdot 10^{-8}$
Test 2 H_2	$4.173 \cdot 10^{-8}$	$5.216 \cdot 10^{-8}$	$6.119 \cdot 10^{-8}$
Test 2 H_2O	$1.285 \cdot 10^{-7}$	$1.065 \cdot 10^{-7}$	$9.462 \cdot 10^{-8}$
Selectivity	2.95	2.06	1.55

CM700 CO	150°C	200°C	250°C
Test 1 CO	$3.896 \cdot 10^{-8}$	$4.181 \cdot 10^{-8}$	$4.124 \cdot 10^{-8}$
Test 1 H_2O	$1.078 \cdot 10^{-7}$	$8.885 \cdot 10^{-8}$	$8.224 \cdot 10^{-8}$
Test 2 CO	$3.951 \cdot 10^{-8}$	$4.138 \cdot 10^{-8}$	$4.107 \cdot 10^{-8}$
Test 2 H_2O	$1.029 \cdot 10^{-7}$	$8.782 \cdot 10^{-8}$	$7.629 \cdot 10^{-8}$
Selectivity	2.69	2.12	1.93

Appendix B: steady state in vapor permeation tests

In vapor permeation tests, the time chosen for each experiment was of 2h. Within this timeframe it has been proven that the system is in steady state. With the previous setup in use (liquid water was fed with high pressure pump, instead that with CEM), it was possible to continuously measure the amount of water that was permeating over time. The measurements were taken every 2 minutes. These data points were then plotted vs time, as in Fig. 1:

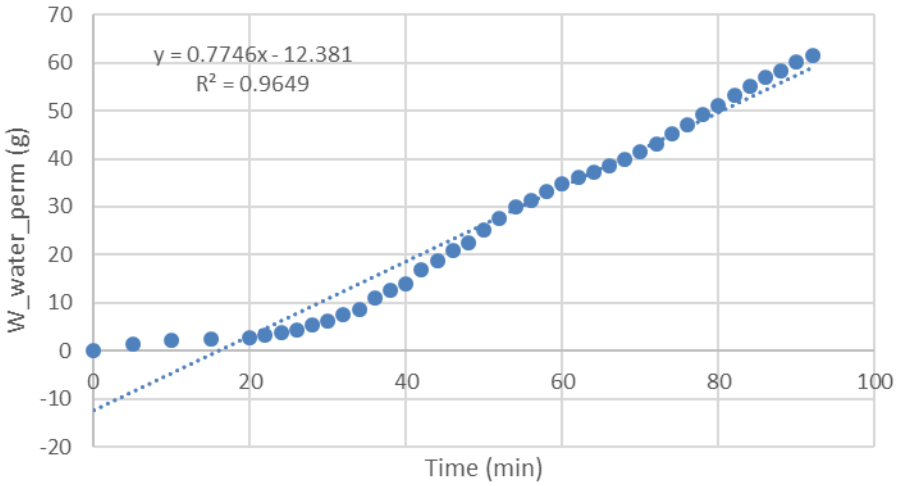

Fig. 1: permeated water weight vs time at 150°C. This graph is taken as an example for the steady state determination.

At the beginning of the experiment, the weight increment is unstable and very low. After a certain time-span, the increment starts to increase over time. Moreover, it is constant within the interval between each measurement. This is represented in the graph in Fig. 1, where the initial curve tends to approximate a steady state line. By doing the data fitting, it is possible to find the intercept with the x-axis. The x-value where the water weight is zero, it is what is called time-lag.

The time-lag is defined as the time necessary to the system to reach approximatively steady state. Usually, the error introduced by the unsteady state prior to the system time-lag is negligible when the experimental total time is three times the time-lag or more. In this case, the highest time-lag observed was around 15 minutes at 150°C. Therefore, the choice to have a 2h long experiment assures both the system in steady state and the negligible error of unsteady state system during the calculations.

Appendix C: activation energy calculation for membrane permeation

When dealing with solution-diffusion mechanism driven by a difference in partial pressure, the permeation can be defined as:

$$\wp = DS$$

where D is the diffusivity coefficient and S the solubility coefficient. The temperature dependency of both diffusivity and solubility coefficients can be expressed as an Arrhenius type relationship, as:

$$D = D_0 \exp\left(-\frac{E_D}{RT}\right)$$

$$S = S_0 \exp\left(-\frac{\Delta H}{RT}\right)$$

Therefore, the permeation can be expressed as:

$$\wp = \wp_0 \exp\left(-\frac{Ea}{RT}\right)$$

where Ea is the activation energy of the permeation. This energy is given by the sum of both energy contributions, E_D and ΔH. $\wp_0$ is equal to D_0*S_0. [46]

Appendix D: indirect model validation from Portha et al. [44]

In their study, Portha et al. [44] also included experimental section to validate the model. These experimental data points are also used for this validation. It is possible to notice that some deviation is present, which is the same deviation obtained from the authors of the study.

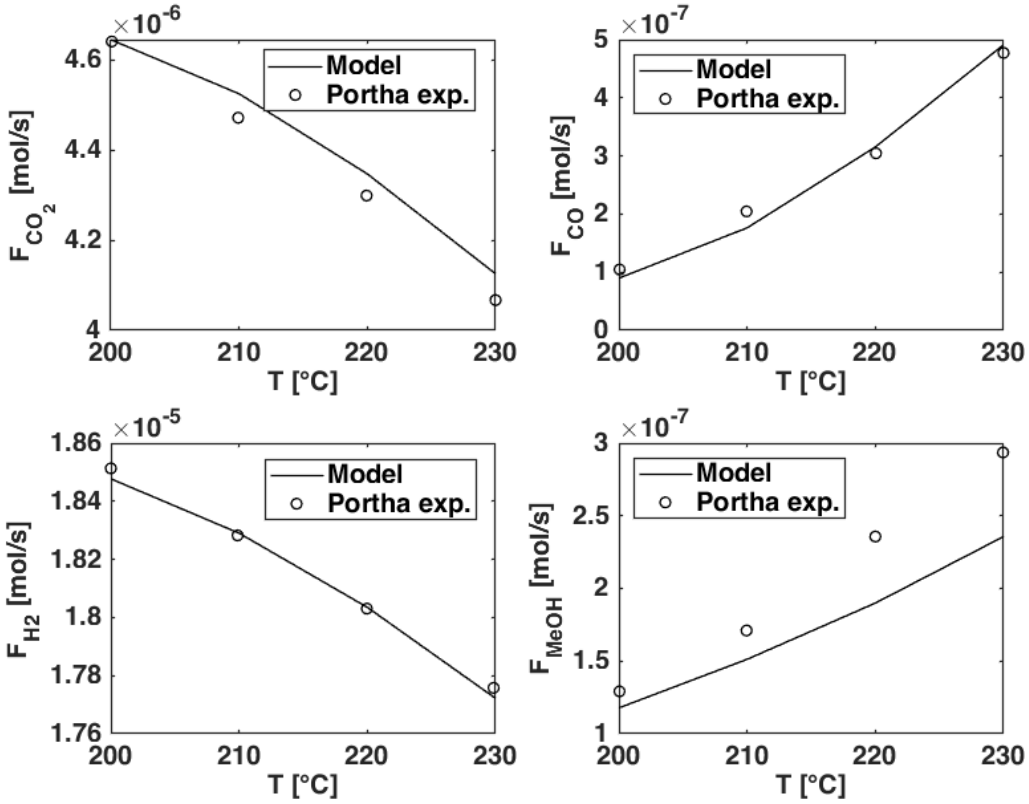

As it is possible to see, the Methanol flowrate has the highest deviation when temperature is increased. However, the model stands for the operating temperature of this study, which is 200°C.